



Norwegian University of
Science and Technology

Voltage control for optimization of power transmission for a long subsea HVAC cable

**Christen Paulov
Engebretsen**

Master of Science in Electric Power Engineering

Submission date: June 2017

Supervisor: Elisabetta Tedeschi, IEL

Co-supervisor: Gilbert Bergna Diaz, IEL

Norwegian University of Science and Technology
Department of Electric Power Engineering

Abstract

The objective of this thesis is to make a dynamic system representation of a long HVAC subsea cable, to investigate the use of controlling the operation voltage to optimize the active power transmission of the cable.

The dynamic representation is based on the simplified model presented in “*Variable Transmission Voltage for Loss Minimization in Long Offshore Wind Farm AC Export Cables*” [1]. The paper is a static analysis investigating the potential of minimizing the losses for a long HVAC cable, by using either fixed or variable voltage control.

The system presented in [1] consists of an offshore wind farm (OWF) connected to a grid onshore through an AC cable. The analysis of the system only considers the cable side of the system by representing the OWF and the grid, with their respective transformers with on-line tap-changers (OLTC), as voltage sources, V_1 and V_2 respectively. This is made possible by assuming the transformers as ideal. The operation voltage is controlled by the voltage source V_2 . The variable operation voltage is optimized to the produced active power from V_1 . By continuously adjusting the voltage scaling to the instantaneous active power production, the operation current is kept within the operation limit of the cable. The result of the analysis is that the cable losses are minimized by controlling the operation voltage. The variable operation voltage is found to have the highest loss reduction.

The dynamic representation of [1] made in the thesis, substitutes the transformers with OLTC, with back-to-back DC converters. The voltage regulation will then be faster. The dynamic representations for fixed and variable operation voltage were made in Simulink. The voltage source representing the OWF V_1 , was made as a voltage source with a voltage source converter (VSC) as a control loop to control the active power output of the voltage source. The voltage source representing the grid V_2 , was made as a voltage source with a fixed input for the fixed operation voltage model. The variable operation voltage model had a control loop, which adjusted the operation voltage based on the active power received at the grid side of the cable to create a more realistic model. It did not however continuously adjust the voltage scaling. The performance and viability of the system were investigated for several power production and fixed voltage levels. The performance was considered by calculating the cable efficiency. The viability of the system was considered by measuring the operation current and voltage to see if they were within the cable’s operation limits.

Most of the simulations were found to have exceeded the current limit of the cable, and none of the simulations had as high cable efficiency as in [1]. The only simulations that did not exceed the current limit was the low production levels for variable operation voltage and low fixed operation voltage. The low fixed operation voltage simulations were found to have the highest operation area for power produced and the highest cable efficiency. The difference in results between the simulations in this Thesis and [1] can be explained by the high charging currents, which suggest that the cable selected for the simulations is not equal to the one in [1].

The use of voltage control to optimize the power transmission was however found to work as the simulations showed that low operation voltages gave the highest cable efficiency for low production and high operation voltage gave the highest cable efficiency for high production.

Sammendrag

Formålet med denne masteroppgaven var å lage en dynamisk systemrepresentasjon av en lang HVAC-undersjøiskabel for å undersøke bruken av å styre driftsspenningen for å optimalisere kabelens aktive effektoverføring.

Den dynamiske representasjonen er basert på den forenklete modellen presentert i “*Variable Transmission Voltage for Loss Minimization in Long Offshore Wind Farm AC Export Cables*” [1]. Oppgaven er en statisk analyse som undersøker potensialet for å minimere effekttapet for en lang HVAC-kabel, ved hjelp av enten variabelregulering av driftsspenningen eller konstant driftsspenning.

System presentert i [1] består av en havvindmøllepark som er koblet til et kraftnett på land gjennom en AC-kabel. Når systemet analyseres vurderes bare kabelsiden av systemet. Dette er mulig ettersom havvindmøllepark og kraftnettet på land sammen med deres respektive regulerbare transformator blir representert som regulerbare spenningskilder, V1 og V2. Dette er tillatt ved å anta at transformatorene er ideelle. Driftsspenningen styres av spenningskilden V2. Den variable driftsspenningen er optimalisert til den produserte aktive effekten fra V1. Driftsstrømmen blir holdt innenfor driftsgrensen til kabelen ved å kontinuerlig justere spenningsskaleringen til den aktive effektproduksjonen til spenningskilden V1. Resultatet av analysen viser at kabeltapet kan minimeres ved å kontrollere driftsspenningen. Det høyeste reduksjonen av effekttap er funnet for bruk av variabel driftsspenning.

I den dynamiske representasjonen av systemet presentert i [1] blir de regulerbare transformatorene erstattet med back-to-back DC-omformere. Spenningsreguleringen vil da bli raskere. De dynamiske representasjonene for konstant og variabel driftsspenning ble laget i Simulink. Spenningskilden som representerer havvindmøllepark V1, ble laget som en spenningskilde, som med en spenningskildeomformer som en kontrollsløyfe styrer spenningskildens aktive effektproduksjon. Modellen av spenningskilden V2 ble konstruert som en spenningskilde som mottar en konstant verdi som driftsspenningen justeres etter for den konstante driftsspennings modellen. Modellen for spenningskilden V2 med variabelregulering av driftsspenningen ble konstruert med en kontrollsløyfe som justerte driftsspenningen basert på den aktive effekten som ble mottatt på kraftnett siden av kabelen, for å lage et mer realistisk system. Den justerer derimot ikke spenningsskaleringen kontinuerlig for den produserte effekten. Ytelsen og levedyktigheten til systemet ble undersøkt for flere effektproduksjonsnivåer og forskjellige nivåer for konstant driftsspenning. Ytelsen av systemene ble vurdert etter effektiviteten til kabeloverføringen. Systemenes levedyktighet ble vurdert etter om driftsgrensene til driftsstrømmen og driftsspenningen til kabelen ble opprettholdt.

Resultatet av de fleste simuleringene viste at kabelens driftsgrense for driftsstrøm var oversteget. Videre viste det seg at ingen av simuleringene hadde så høy kabeloverføringseffektivitet som ble funnet i [1]. Det var bare simuleringene for lave effektproduksjonsnivå for variabelregulering av driftsspenningen og lave konstante driftsspenninger som hadde driftsstrøm som ble holde innenfor driftsgrensen til kabelen. Det var simuleringene for lav konstant driftsspenning som viste seg å ha de høyeste operasjonsområde for produsert aktiv effekt og den høyeste effektiviteten for kabeloverføring. Forskjellen mellom resultatene i denne oppgaven og [1] kommer av de høy ladestrømmen funnet i simuleringene av den dynamisk

representasjonen av systemet. Dette tyder på at kablen valgt for den dynamiske representasjonen av systemet er ulik den valgt i [1].

Allikevel viste simuleringene at bruken av spenningsregulering for å optimalisere effektoverføringen til en HVAC-kabel fungerer. Ettersom at simuleringene viste at lav driftsspenning resulterte i høy effektivitet for kabeloverføringen av aktiv effekt for lav effektproduksjon og høy driftsspenning ga høy effektivitet for kabeloverføringen av aktiv effekt for høy effektproduksjon.

Preface

The thesis: “*Voltage control for optimization of power transmission for a long subsea HVAC cable*” was written at the Norwegian University of Science and Technology, Faculty of Engineering Science and Technology, Department of Electric Power Engineering.

All work has been conducted at NTNU, Trondheim. The work that has been performed has been based on the paper: “*Variable Transmission Voltage for Loss Minimization in Long Offshore Wind Farm AC Export Cables*” [1].

I would like to thank my supervisors at NTNU, Professor Elisabetta Tedeschi and PhD Gilbert Bergna for their counselling and advice when writing this thesis.

Trondheim
8th of June 2017
Christen Paulov Engebretsen

Table of content

Abstract	i
Sammendrag	iii
Preface	v
List of Figures	ix
List of Tables.....	xi
Abbreviations	xiii
1 Introduction.....	1
1.1 Problem statement	2
1.2 State of the art.....	2
1.3 Structure.....	2
2 System description	3
2.1 HVAC cable	3
2.2 Reactive compensation	5
2.3 Simplification of system.....	5
2.4 Cable efficiency	7
2.5 Voltage scaling	8
2.6 Optimal operating voltage	9
2.7 Operation strategies	10
2.8 Summation of results	12
2.9 Replication of work	13
3 Design of dynamic model	15
3.1 Model of voltage source V_1	15
3.1.1 Voltage source converter.....	16
3.2 Model of voltage source V_2	20
3.3 Model of HVAC cable.....	20
4 Simulink model of dynamic system.....	21
4.1 Design of voltage source V_1	21
4.1.1 Design of voltage source converter.....	22
4.2 HVAC cable selection	26
4.3 Design of voltage source V_2	26
4.4 Power Measurement	28
4.5 Powergui	28
5 Results.....	29
5.1 Active power production test simulation.....	29

5.2	Cable efficiency	31
5.3	Summation of results	35
6	Conclusion	37
7	Bibliography	39
	Appendix	I
	Appendix A: Matlab scripts and functions	III
	Appendix A1	III
	Appendix A2	IV
	Appendix A3	V
	Appendix A4	VI
	Appendix A5	VII
	Appendix A6	VIII
	Appendix B: Results from simulations	IX
	Appendix B1	IX
	Appendix B2	XII

List of Figures

Fig. 1. Connection of wind farm to shore. [1].....	3
Fig. 2. Typical structure of three-core armoured XLPE cable. [9]	3
Fig. 3. Π -type equivalent circuit of XLPE cable. [9]	4
Fig. 4. Ferranti effect in transmission line. [5].....	4
Fig. 5. Electrical equivalent with cable represented by exact pi-equivalent. [1]	6
Fig. 6. Cable efficiency as function of wind farm voltage scaling, $\xi = 1 \cdot e^{j\beta}$ for different cable lengths. [1].....	8
Fig. 7. Cable efficiency of 200 km cable as function of wind farm voltage scaling, $\xi = \alpha \cdot e^{j\beta}$. [1]	9
Fig. 8. Optimal cable operating voltage V_2 as function of wind farm instantaneous production P_{wf} , for maximum efficiency for the 200 km cable. The asterisk and the circle denote the operating voltage V_2 at which the cable rated current and rated voltage are exceeded, respectively. [1].....	10
Fig. 9. Cable efficiency for 200 km cable as function of wind farm instantaneous active power production. Parameter: Cable operating voltage V_2 . [1]	11
Fig. 10. Optimal cable operating voltage as function of wind farm instantaneous active power production. Parameter: Cable length. [1]	11
Fig. 11. Cable efficiency as function of wind farm instantaneous active power production. Solid lines: Operation at optimal (variable) voltage. Dashed lines: operation at 1.0 p.u. fixed voltage.	12
Fig. 12. Replication of Fig. 6. Cable efficiency as function of wind farm voltage scaling, $\xi = 1 \cdot e^{j\beta}$ for different cable lengths.....	13
Fig. 13. Replication of Fig. 7. Cable efficiency of 200 km cable as function of wind farm voltage scaling, $\xi = \alpha \cdot e^{j\beta}$	13
Fig. 14. Back-to-back DC converter. [14].....	15
Fig. 15. Voltage source converter, with and outer power controller and inner current controller. [17].....	16
Fig. 16. Inner current controller. [17].....	18
Fig. 17. Simplified block diagram of the inner current controller. [16].....	18
Fig. 18. Outer power controller, with only active power control. [17]	19
Fig. 19. Model of the HVAC system developed in Simulink.	21
Fig. 20. Simulink model of voltage source V_1	22
Fig. 21. Simulink model of the inner current controller.....	22
Fig. 22. abc to dq0 conversion of current and voltage.	23
Fig. 23. Simulink model of outer power controller.	24
Fig. 24. Incorrect tuning of the outer power controller.	25
Fig. 25. Correct tuning of the outer power controller.	26
Fig. 26. Simulink model of the voltage source V_2 with fixed operation voltage.	27
Fig. 27. Simulink model of the voltage source V_2 with variable operation voltage.	27
Fig. 28. Simulink model of the power measurement block shown in Fig. 19.....	28
Fig. 29. 1.0 p.u. active power production from V_1 . With 1.0 p.u. fixed operation voltage at V_2	29
Fig. 30. 1.0 p.u. active power production from V_1 . With variable operation voltage at V_2	30
Fig. 31. Active power received at grid for 1.0 p.u. production by V_1 . With 1.0 p.u. fixed operation voltage at V_2	30

Fig. 32. Active power received at grid for 1.0 p.u. production by V_1 . With variable operation voltage at V_2 .	30
Fig. 33. Operation voltage of voltage source V_2 with variable operation voltage for 1.0 p.u. production by V_1 .	31
Fig. 34. Calculated cable efficiencies for all the fixed operation voltage model simulations, within the efficiency area zero to 1. * and · denote that the operation current is within or exceeds the cable's current limit, respectively.	32
Fig. 35. Calculated cable efficiency for the variable operation voltage model simulation, within the efficiency area zero to 1. * and · denote that the operation current is within or exceeds the cable's current limit, respectively.	32
Fig. 36. Cable efficiency as a function of p.u. power production by V_1 for 0.2 p.u. fixed operation voltage at V_2 , within the efficiency area zero to 1. * and · denote that the operation current is within or exceeds the cable's current limit, respectively.	33
Fig. 37. Cable efficiency as a function of p.u. power production by V_1 for 0.3 p.u. fixed operation voltage at V_2 , within the efficiency area zero to 1. * and · denote that the operation current is within or exceeds the cable's current limit, respectively.	33
Fig. 38. Cable efficiency as a function of p.u. power production by V_1 for 0.9 p.u. fixed operation voltage at V_2 , within the efficiency area zero to 1. * and · denote that the operation current is within or exceeds the cable's current limit, respectively.	34
Fig. 39. Cable efficiency as a function of p.u. power production by V_1 for 1.0 p.u. fixed operation voltage at V_2 , within the efficiency area zero to 1. * and · denote that the operation current is within or exceeds the cable's current limit, respectively.	34
Fig. 40. Operation voltage as a function of p.u. power production by V_1 for variable operation voltage at V_2 , within the efficiency area zero to 1. * and · denote that the operation current is within or exceeds the cable's current limit, respectively.	35
Fig. 41. Alignment for constant reference current equal to 1.0 p.u. and control current, i_d .	IX
Fig. 42. Alignment for constant reference current equal to 1.0 p.u. and control current, i_q .	IX
Fig. 43. Alignment for varying reference current (0.3-1.0 p.u.) and control current, i_d .	X
Fig. 44. Alignment for varying reference current (0.3-1.0 p.u.) and control current, i_q .	X
Fig. 45. Alignment for varying reference current (0.3-1.0 p.u.) and control current, i_d . With reference i_q set at constant value equal to zero.	XI
Fig. 46. Alignment for constant reference current equal to zero and control current, i_q . With varying reference current i_d (0.3-1.0 p.u.).	XI

List of Tables

TABLE I. Cable parameters (50 Hz) and characteristics. [1] [10]	5
TABLE II. Pseudocode for determination of operating voltage for maximum efficiency for each level of wind farm production. [1]	9
TABLE III. Result of Matlab TM script for a 200 km cable. [1].....	9
TABLE IV. Result of optimal operation voltage script, <i>opt_V_scaling</i> (appendix A4).....	14
TABLE V. Calculated p.u. values from script (appendix A5).....	24
TABLE VI. Calculated K_{iICC} and K_{pICC} from script (appendix A5).	24
TABLE VII. Calculated cable efficiency for fixed operation voltage model simulation. The red numbers mark the simulations where the current exceeds the cable's current limit.....	XII
TABLE VIII. Calculated efficiency for the simulation of the variable operation voltage model. The red number mark the simulations where the current exceeds the cable's current limit.	XII

Abbreviations

ICC	Inner current controller
OLTC	On-line tap-changers
OPC	Outer power controller
OWF	Offshore wind farm
p.u.	Per unit
SR	Shunt reactor
VSC	Voltage source converter

1 Introduction

There has been increased investment in offshore wind the last years, this development is continuing. Placing wind farms offshore is preferred over onshore, as the wind is stronger, steadier, less turbulent and blow more frequently. In addition, it is difficult to find good sites onshore, due to densely populated areas and the strict environmental constraints. The production potential of an offshore wind farm (OWF) increases the longer it is placed from shore. [2]

Most OWFs are as of today, connected to onshore grids by HVAC cables, as HVDC cables are more expensive due to the necessity of converter stations and higher operation costs. HVDC cables are complex to operate, as they have less control and protection equipment compared to HVAC cables. HVDC cables are however for cable connections over 50 km more economical feasible than HVAC cables, as there are substantial cable losses due to the HVAC cable's capacitive characteristics. [2], [3]

The capacitive characteristic of the HVAC cable is a result of the potential difference between the conductors in the cable, which is caused by the high dielectric strength from the insulation between the conductors and the conductors close proximity to each other. The capacitances between the conductors will charge and discharge, when the conductors are applied alternating voltage, this results in charging currents. The charging currents will create a voltage drop over the line inductance of the cable, resulting in the voltage on the receiving side being higher than the voltage on the sending side. This effect increases with the cable's length, as the conductors are more exposed to each other. The charging currents limit the active power transmission and length of the cable. [4], [5]

The charging currents can be reduced by controlling the operation voltage of the cable. This thesis will investigate the use of controlling the operation voltage at the grid side to increase the cable efficiency and thereby increasing the HVAC cable's active power transmission. The use of both fixed and variable voltage at the grid side will be investigated. [1]

The work is based on the paper: "*Variable Transmission Voltage for Loss Minimization in Long Offshore Wind Farm AC Export Cables*" [1]. Which is a static analysis, investigating the potential of minimizing the losses of a long HVAC cable by controlling the operation voltage, as either fixed or variable voltage. The variable operation voltage minimizes the cable losses by adjusting to the wind farm's instantaneous produced power. The system in [1] is only considering the cable side of the system, this is made possible by representing the OWF and the grid with their respective shunt reactor (SR) and transformer with on-line tap-changers (OLTC) as adjustable voltage sources.

1.1 Problem statement

The goal of this thesis is to make a dynamic representation of the simplified system presented in “*Variable Transmission Voltage for Loss Minimization in Long Offshore Wind Farm AC Export Cables*” [1]. To investigate the viability and performance of controlling the operation voltage of a 200 km long HVAC cable, to optimizing the cable efficiency for variation in production level by the OWF.

1.2 State of the art

There is a lot of literature on the topic of extending the transmission capability of long HVAC cables. Most papers written on the subject are about the use of SRs to increase the active power transmission of the cables, by optimizing a suitable shunt compensation for the cable connection. The system is then evaluated through steady state and transient simulations. Often the HVAC-solution is compared with HVDC- solution, where the technical solutions and costs are compared. In most cases, HVDC is found to be the best solution for longer cable lengths, as the cost is lower. [6]

Using low frequency is another solution. This will reduce both the charging current and the skin effect of the conductors. This type of technology is however not in use, as it has not yet been qualified for use. Another disadvantage is the increased weight and volume of the magnetic components and the necessity of converter stations. [1], [7]

This thesis will investigate the use of controlling the operation voltage of a HVAC cable with back-to-back DC converters, to increase the cable’s active power transmission. The operation voltage will be controlled at the grid side, either as fixed or variable operation voltage. The variable operation voltage is regulated to the active power production by the OWF, by measuring the active power received at the grid side to make a more realistic model. The back-to-back DC converters enables the OWF and grid to be decoupled from the cable side of the system. It also enables the faster voltage regulation than the more traditional transformers with OLTC. [8]

When investigating the dynamic model, that is to be made based on the system in [1], the back-to-back DC converters will replace the transformers with OLTC. The system will then only consider the cable side of the system.

1.3 Structure

Chapter 2 describes the system presented in [1]. This includes the concept and simplifications made for analyzing the system and the results. There is also a subchapter about replicating some of the work. Chapter 3 is about the design of the dynamic system, which includes the theory of producing the different system parts of the system. Chapter 4 is about the procedure of making the model in Simulink. In chapter 5 the results of the simulations for the fixed and variable voltage models will be presented. In chapter 6 the conclusion of the performance and viability of the system will be presented.

2 System description

The dynamic model that is to be created to investigate the use of voltage regulation for increasing the active power transmission of an HVAC cable is based on the system presented in “*Variable Transmission Voltage for Loss Minimization in Long Offshore Wind Farm AC Export Cables*” [1]. In this chapter, the system investigated in [1] will be presented with elaboration on the equipment used in the system. Further, the simplifications and limitations made for analyzing the system will be presented, followed by the results. All of this is of interest for the further work of making a dynamic model of the system.

The analysis of the system investigated in [1] is a static analysis, which investigates the use of continuously adjusting the voltage at the grids to the OWF’s produced power to minimize the losses of an HVAC cable. The system is presented in Fig. 1.

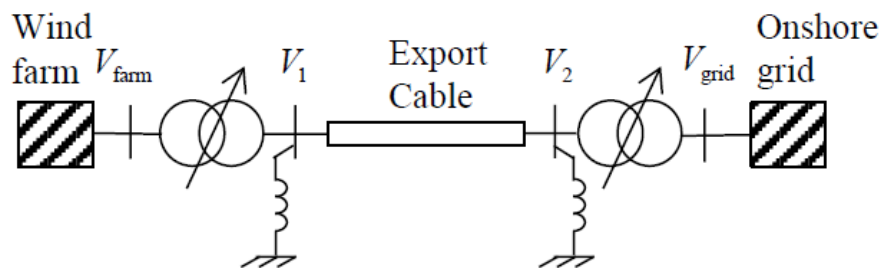


Fig. 1. Connection of wind farm to shore. [1]

The system considers an OWF connected to a grid at land by an AC cable. The OWF and onshore grid are decoupled from the cable side by transformers with OLTC. The reactive power is compensated by the indicated SRs on each side of the cable, with support from the transformers.

2.1 HVAC cable

A typical structure of an HVAC cable is shown in Fig. 2. There is a high dielectric strength from the insulation between the conductors creating potential difference between the three conductors. This cause the conductors to charge. This creates a capacitive characteristic between the conductors. The capacitances are a result of the charge per unit (p.u.) of potential difference between the conductors. [4]

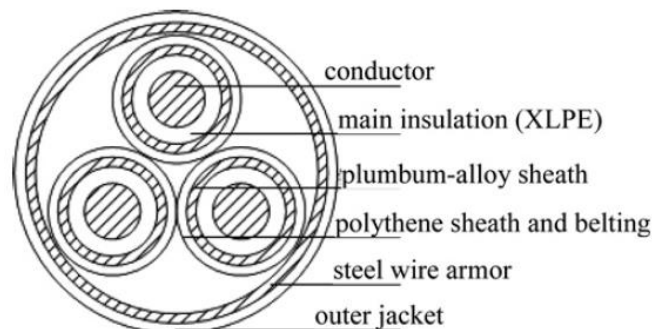


Fig. 2. Typical structure of three-core armoured XLPE cable. [9]

When the conductors are applied an alternating voltage, the capacitance will alternate between charging and discharging, resulting in charging currents.

The HVAC cable is represented by its exact PI- equivalent circuit, shown in Fig. 3.

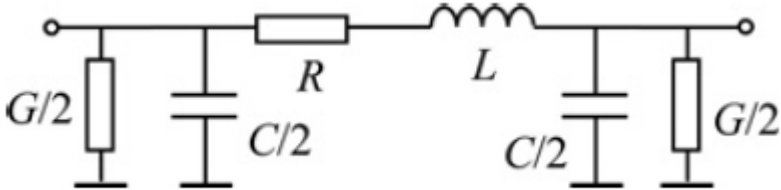


Fig. 3. Π -type equivalent circuit of XLPE cable. [9]

Where R, L, C and G represent the cable’s line resistance, line inductance, shunt capacitance and shunt conductance respectively.

When the charging current drawn by the shunt capacitance of the HVAC cable, is higher than the load current at the receiving side the Ferranti effect will occur, illustrated in Fig. 4. The Ferranti effect is the increase in voltage at the receiving side of the cable, which is a result of the voltage drop over the line inductance caused by the charging currents. I_c , V_s , V_r and R represents the charging current, sending voltage, receiving voltage and line the resistance. [4], [5]

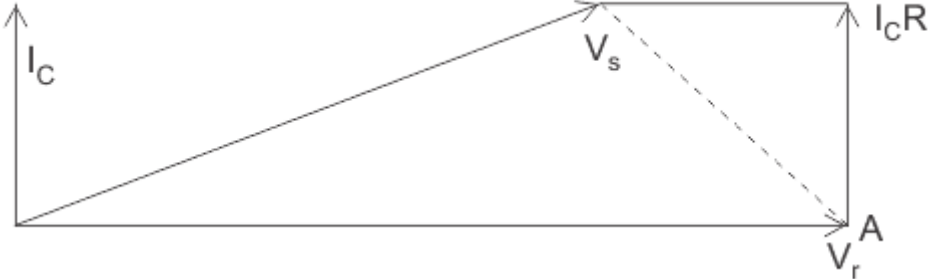


Fig. 4. Ferranti effect in transmission line. [5]

When the OWF is at high production, the charging currents increases. The operation current will then increase and the rated current of the cable will then be exceeded. This results in limiting the active power transmission of the cable, and thereby the cable length. [1]

The cable characteristics of the AC cable presented in [1] is given in TABLE I.

TABLE I. Cable parameters (50 Hz) and characteristics. [1] [10]

Nominal voltage [kV]	220
Cable section [mm ²]	1000
R [Ω /km]	0.048
L [mH/km]	0.37
C [μ F/km]	0.18
G [S/km]	0
Nominal current [A]	1055

2.2 Reactive compensation

A solution to increasing the active power transmission of a HVAC cable is to decrease the operation voltage of the cable. It is observed that the charging currents then will decrease. [1], [3]

The reactive compensation solutions provided for the system in [1] is the SRs, the OWF and the transformers on each side. The SRs counteract the cables capacitive characterizes by absorbing the reactive power from the cable, reducing the voltage and thereby also the charging currents. The transformers in addition to voltage transformation, are also able to control the operation voltage of the cable and the reactive power flow. The control of voltage and reactive power is enabled by the OLTC. OLTC are used when the voltage ratio is changing frequently. By controlling the operation voltage of the cable, the current and voltage is maintained within the cable's limitations. Based on the OWF's active power production the OLTC adjust the operation voltage, to increase the cable efficiency. The transformers OLTC capability is assumed to be $\pm 15\%$. [1], [4]

2.3 Simplification of system

To analyze the system presented in Fig. 1 some simplifications are done in [1]. First the transformers on each end is to be considered as ideal. The onshore voltage V_{grid} is assumed to be fixed at 380 kV. The ratio between the onshore and cable onshore voltage V_2 is represented by k . The cable onshore voltage is then equal to (1).

$$V_2 = k \cdot V_{grid} \quad (1)$$

The offshore voltage on the cable side V_1 is allowed to exceed the cable voltage V_2 on the onshore by 10%. The permitted operation area of the voltage on this side is specified by (2).

$$V_1 = V_2 \cdot \alpha e^{j\beta} \quad (2)$$

Where α is the ratio between the voltage amplitude at the farm side V_1 and grid side V_2 . β is the difference in phase angle between the voltages at the two ends of the cable.

As the transformers are considered ideal, only the cable side voltages are considered further. These are represented as voltage sources where V_1 represents the transformer with OLTC, wind turbine converters and reactive power compensation equipment on the offshore side. V_2 represents the transformer with OLTC on the grid side and the onshore grid.

The series impedance and shunt admittance is calculated by (3) and (4) from the cable characteristics in TABLE I.

$$Z = R + j\omega L \quad (3)$$

$$Y = G + jC \quad (4)$$

From the series impedance and shunt admittance, the surge impedance Z_C (5) and propagation constant γ (6) can be calculated. The surge impedance is the ratio of the voltage and current of a wave travelling along the line, with no reflection. [11] The propagation constant describes the behavior of an electromagnetic wave along a transmission line. [12]

$$Z_C = \sqrt{\frac{Z}{Y}} \quad (5)$$

$$\gamma = \sqrt{ZY} \quad (6)$$

The calculated surge impedance and propagation constant are inserted into (7) together with the cable length l to obtain the cable admittance matrix.

$$\Pi = \begin{bmatrix} \frac{\coth(\gamma l)}{Z_C} & \frac{-1}{Z_C \sinh(Z_C)} \\ -1 & \frac{\coth(\gamma l)}{Z_C} \\ \frac{1}{Z_C \sinh(Z_C)} & \frac{-1}{Z_C} \end{bmatrix} \quad (7)$$

The product of the simplifications made is the model in Fig. 5.

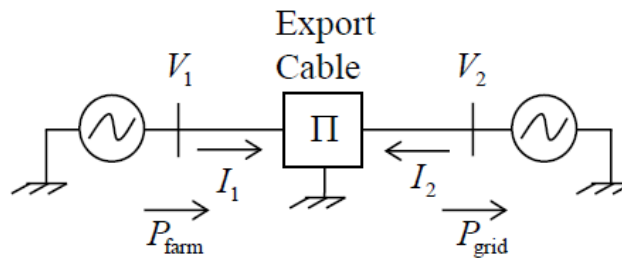


Fig. 5. Electrical equivalent with cable represented by exact pi-equivalent. [1]

2.4 Cable efficiency

The goal of [1] is to minimize the AC cable's transmission losses. The cable efficiency is the ratio of the received active power at the grid and the produced active power from the wind farm (8). Where P_{farm} is the active power produced by the OWF and P_{grid} is the active power received at the grid side.

$$\eta = \frac{P_{grid}}{P_{farm}} \quad (8)$$

The active power at each end can be calculated by (9) and (10). Where V_1 , V_2 , I_1 and I_2 are the terminal voltages and currents and each end of the cable. Re is the real part of the complex number and $*$ represents the conjugate of the complex number.

$$P_{farm} = \sqrt{3}Re\{V_1 I_1^*\} \quad (9)$$

$$P_{grid} = -\sqrt{3}Re\{V_2 I_2^*\} \quad (10)$$

From the simplified model, the admittance matrix from (7), together with the terminal voltages can be used to calculate the terminal currents (11).

$$[I_1 \ I_2]^T = \Pi \cdot [V_1 \ V_2]^T \quad (11)$$

The voltage scaling between the wind farm side and grid side in (2) can be represented by ξ (12).

$$\xi = \alpha \cdot e^{j\beta} \quad (12)$$

From (2), (7) and (12), (11) can be rewritten as (13). Only the voltage on the grid side is now considered when calculating the terminal currents.

$$\begin{bmatrix} I_1 \\ I_2 \end{bmatrix} = \begin{bmatrix} A & B \\ B & A \end{bmatrix} \begin{bmatrix} \xi V_2 \\ V_2 \end{bmatrix} \quad (13)$$

By inserting the currents calculated from (13) into (9) and (10), one gets the active power for the OWF (14) and grid (15) without considering the current.

$$\begin{aligned} P_{farm} &= \sqrt{3}Re\{\xi V_2 (A\xi V_2 + BV_2)^*\} \\ &= \sqrt{3}Re\{\xi (A\xi + B)^* V_2^2\} \end{aligned} \quad (14)$$

$$\begin{aligned} P_{grid} &= -\sqrt{3}Re\{V_2 (B\xi V_2 + AV_2)^*\} \\ &= -\sqrt{3}Re\{(B\xi + A)^* V_2^2\} \end{aligned} \quad (15)$$

From inserting (14) and (15) into (8), the efficiency is found (16), without considering the voltage.

$$\eta = -\frac{\operatorname{Re}\{(B\xi + A)^*\}}{\operatorname{Re}\{\xi(A\xi + B)^*\}} \quad (16)$$

This shows that the maximum cable efficiency is independent of the operation voltage V_2 , and depending on the voltage scaling ξ . The operating voltage does however determine the transmitted power at a given efficiency.

2.5 Voltage scaling

As the admittance matrix is dependent on cable length, one should adjust the voltage scaling for each unique cable length. Fig. 6 considers the cable efficiency as a function of the scale angle β and constant scaling factor α equal to 1.0 for different cable lengths. It shows that the efficiency decreases with the increase of cable length. The reason for this is that the longest cables only can operate at low voltages, as the charging currents are so high that it will cause the rated current to exceed the nominal value.

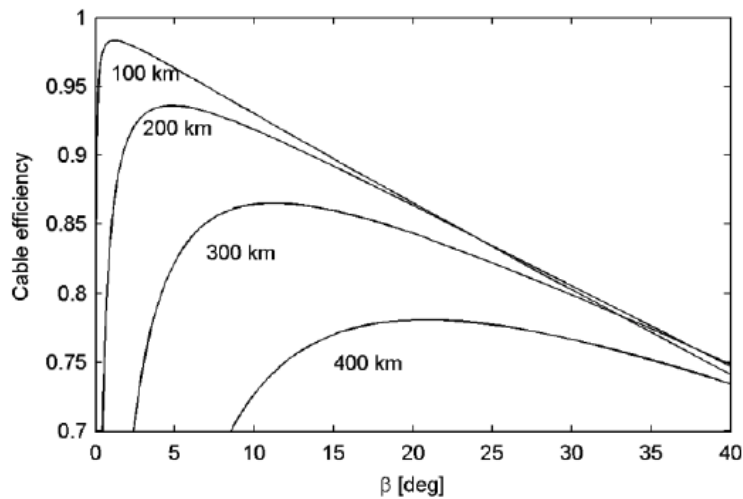


Fig. 6. Cable efficiency as function of wind farm voltage scaling, $\xi = 1 \cdot e^{i\beta}$ for different cable lengths. [1]

Fig. 7 shows the efficiency of a 200 km cable as a function of the scaling angle β with different scaling factor α . One can see that the efficiency for a 200 km cable will not exceed 0.94.

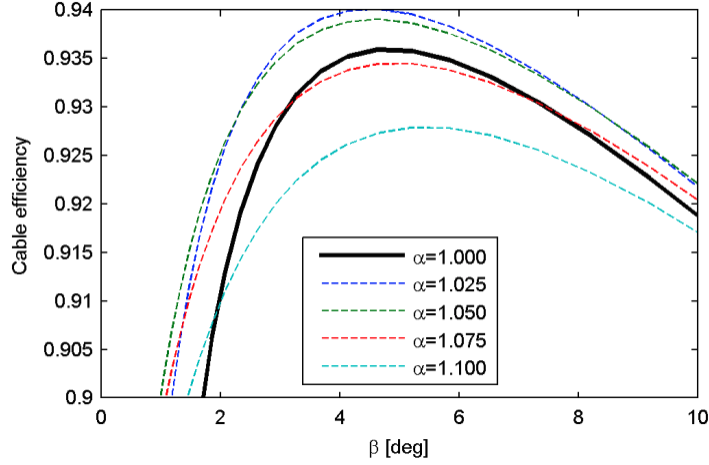


Fig. 7. Cable efficiency of 200 km cable as function of wind farm voltage scaling, $\xi = \alpha \cdot e^{j\beta}$. [1]

Fig. 6 and Fig. 7 shows that by controlling the scaling factor α and scaling angle β the maximum efficiency for each cable length can be achieved. One may also notice that when the cable length reduces, α approach 1.0 and β approaches zero. This corresponds with the voltage at each end to have the same amplitude and zero phase difference. The efficiency should then be close to 1.0.

2.6 Optimal operating voltage

To achieve high power transmission at all times the operation voltage V_2 has to be optimized to the wind farm instantaneous power production.

The optimal operation voltage is calculated by creating a Matlab script with the steps presented in TABLE II.

TABLE II. Pseudocode for determination of operating voltage for maximum efficiency for each level of wind farm production. [1]

1. Read cable length and cable parameters and establish the cable admittance matrix Y_{II} according to (7).
2. Use (11) and (13) to determine A and B in (13).
3. Use MatlabTM optimization routine *fmincon* to find ξ_{opt} that maximizes the efficiency η expressed in (16) together with (12) and the constraints $\alpha \in [1, 1.1]$ and $\beta \in \left[-\frac{\pi}{2}, \frac{\pi}{2}\right]$.
4. Loop through the relevant values for P_{farm} and use (14) and find ξ_{opt} to determine the optimum voltage $V_{2,opt}$ that for each specified P_{farm} maximized the efficiency.

The result of the Matlab script presented in TABLE II for a 200 km cable is presented in TABLE III.

TABLE III. Result of MatlabTM script for a 200 km cable. [1]

α	1.025
β	4.5°
η	0.94

The maximum efficiency found in TABLE III corresponds with the maximum efficiency found in Fig. 6 and Fig. 7.

Fig. 8 shows the maximum permissible operation voltage V_2 as a function of the OWFs instantaneous production, by using the method in TABLE II. The efficiency is kept at 0.94 for the entire curve by adjusting the voltage scaling to the instantaneous production by the OWF.

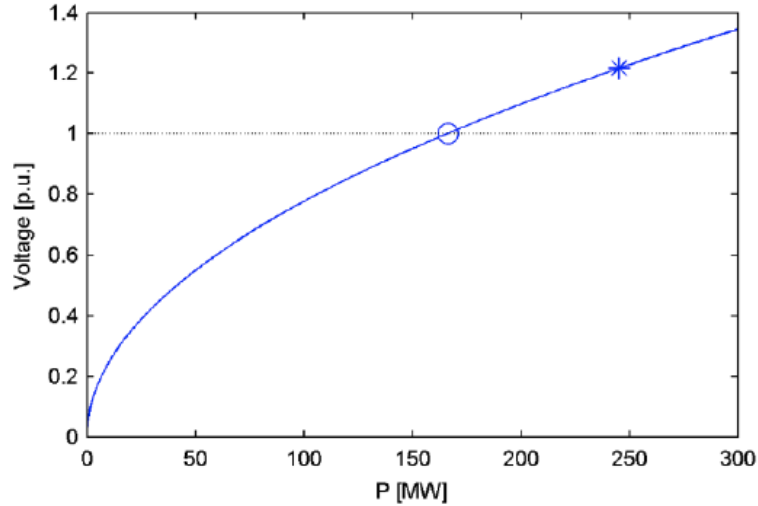


Fig. 8. Optimal cable operating voltage V_2 as function of wind farm instantaneous production P_{wf} , for maximum efficiency for the 200 km cable. The asterisk and the circle denote the operating voltage V_2 at which the cable rated current and rated voltage are exceeded, respectively. [1]

Fig. 8 shows that the operation voltage will be exceeded at a production of 170 MW (marked as O) and that the operation current will be exceeded at 250 MW (marked as *). This means that at high production it is necessary to modify both the operation voltage and the voltage scaling, to not exceed the voltage and current limitations of the cable.

2.7 Operation strategies

The possible operation strategies for the system is either with fixed or variable operation voltage. With fixed operation voltage, V_2 should be lower than the nominal voltage. The operation voltage should be chosen based on the expected production levels, with lower voltages for low production levels and higher voltages for high production. This is confirmed by Fig. 9, which looks at the cable efficiency of a 200 km long cable as a function of the OWF's instantaneous active power production at different voltage operating levels.

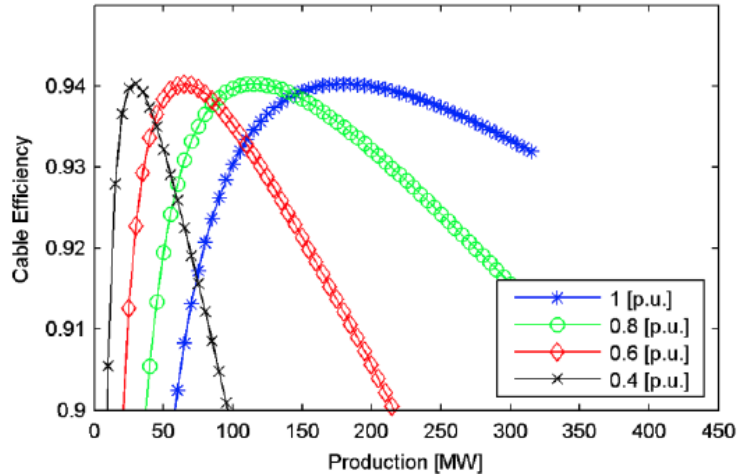


Fig. 9. Cable efficiency for 200 km cable as function of wind farm instantaneous active power production. Parameter: Cable operating voltage V_2 . [1]

A better option is to use variable operation voltage, the operation voltage is then adjusted to the OWF's instantaneous power production. The cable efficiency is then kept at its maximum permissible value at all of the attainable production levels. Fig. 10 shows the cable operating voltage with a range of 0.4 -1.0 p.u. as a function of the wind farm instantaneous active power production for different cable lengths.

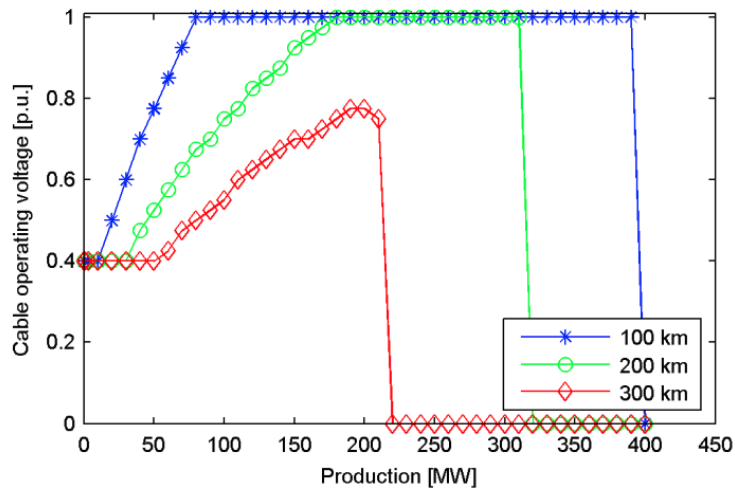


Fig. 10. Optimal cable operating voltage as function of wind farm instantaneous active power production. Parameter: Cable length. [1]

One can see that the voltage increases with the increase of active power production by the OWF.

Fig. 11 shows the cable efficiency as a function of the OWF's instantaneous active power production, where the solid lines represents variable operation voltage and the dashed lines represents 1.0 p.u. fixed operation voltage.

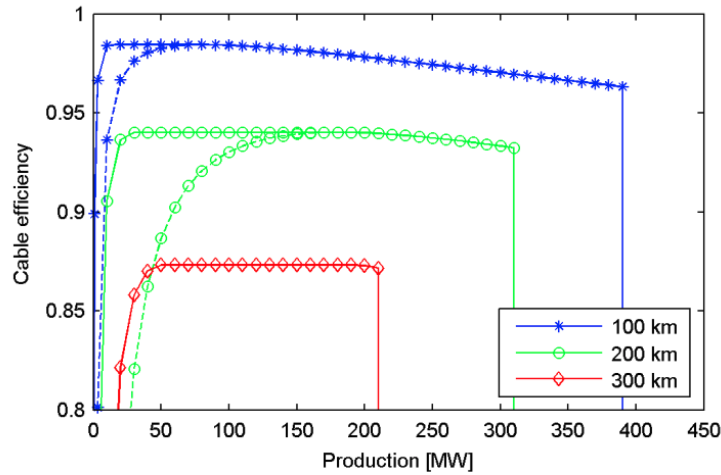


Fig. 11. Cable efficiency as function of wind farm instantaneous active power production. Solid lines: Operation at optimal (variable) voltage. Dashed lines: operation at 1.0 p.u. fixed voltage. Parameter: Cable length. [1]

The result show that the variable operation voltage increases the cable efficiency for lower power production levels. One can see that there are no dashed lines for the 300 km long cable, this is a result of the current limit is exceeded even at low production levels, which means that 1.0 p.u. is not a feasible operation voltage for this cable length.

2.8 Summation of results

The findings of [1] show that the maximum cable efficiency is independent of the operation voltage. The operation voltage will however affect the active power transmission at the given cable efficiency. The maximum efficiency is reached at low power levels when the operation voltage is reduced. By continuously adjusting the operation voltage to the OWF's instantaneous power production the cable efficiency can be increased. For a system consisting of an OWF with the capability of producing 320 MW with a cable connection of 200 km the use of $\pm 15\%$ voltage regulation by the transformers the loss reduction of the system is found to be 9%. By reducing the overall losses with the use of voltage control, the active power transmission will be increased, therefore also increasing the maximum length of the HVAC cable. [1]

2.9 Replication of work

To investigate if the results of the voltage scaling presented in [1] was accurate, Fig. 6 and Fig. 7 were to be replicated. The replication of the figures was done in Matlab.

First, some basic scripts for the cable parameters data from TABLE I, the calculation of admittance matrix and the conversion from polar coordinates to Cartesian coordinates for the voltage scaling were made in Matlab (appendix A1). The necessity of converting the α - and β -value of the voltage scaling to Cartesian coordinates is that Matlab only calculates in radians. From these basic scripts, further calculations could be performed easily. The focus was then directed at trying to replicate the figures Fig. 6 and Fig. 7. The procedure of replicating the figures are presented in the scripts *cable_efficiency_var_cable_length* (appendix A2) and *cable_efficiency_var_alpha* (appendix A3).

The replication of Fig. 6 and Fig. 7 are presented as Fig. 12 and Fig. 13.

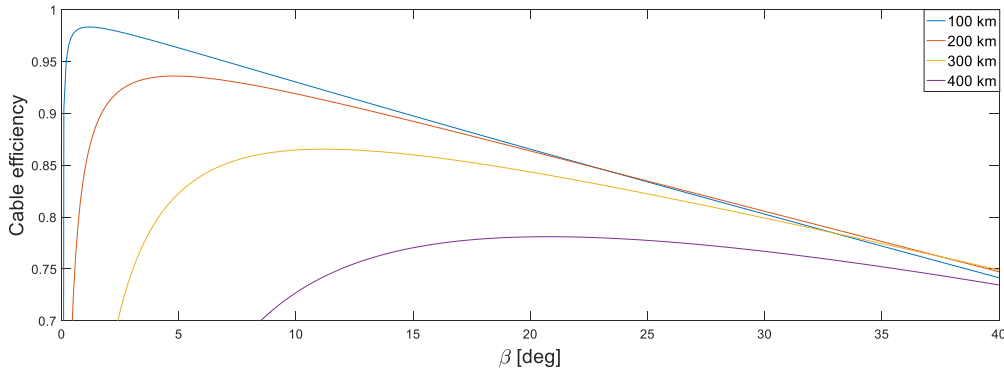


Fig. 12. Replication of Fig. 6. Cable efficiency as function of wind farm voltage scaling, $\xi = 1 \cdot e^{j\beta}$ for different cable lengths.

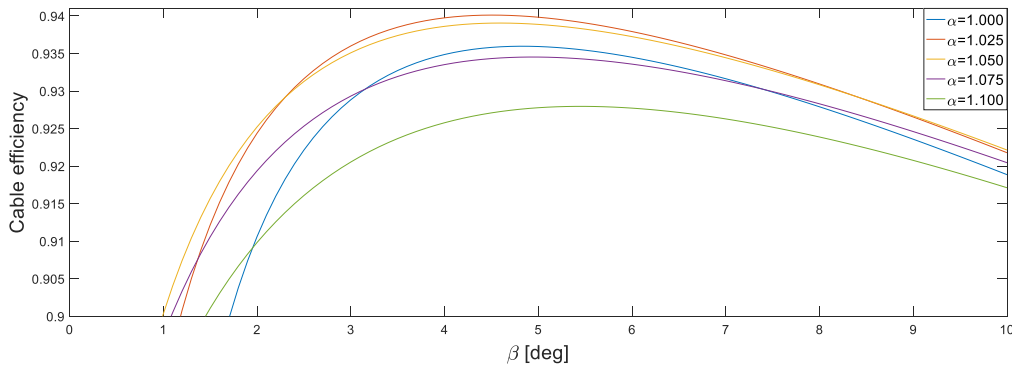


Fig. 13. Replication of Fig. 7. Cable efficiency of 200 km cable as function of wind farm voltage scaling, $\xi = \alpha \cdot e^{j\beta}$.

Both of these figures are equal to the ones presented in the [1], the results of the voltage scaling are therefore found to be the same.

Further, the method of optimizing the operation voltage to the instantaneous active power production of the OWF presented in TABLE II was reproduced. This would enable the

possibility of creating a dynamic model, which regulates the voltage on the grid side to the instantaneous active power production of the OWF.

The method of optimized operation voltage for maximizing the cable efficiency for the production level of the OWF as in TABLE II was made as the script *opt_V_scaling* (appendix A4). The script considers a 200 km long cable, and optimize the voltage scaling for the given cable length to find the highest efficiency. The result of the script is presented in TABLE IV.

TABLE IV. Result of optimal operation voltage script, *opt_V_scaling* (appendix A4).

α	1.0343
β	4.353
η	0.9403

The voltage scaling from TABLE IV differ from the found in TABLE III, the deviation comes most likely from the desire to operate with “finer” numbers. The difference in the calculated efficiency is so small that it can be disregarded, it is therefore concluded that the voltage scaling is found be the same.

Step 4 from TABLE II was however not fulfilled. Step 4 states that the operation voltage $V_{2,opt}$ is calculated by (14) with the input of produced power from the OWF P_{farm} and optimal voltage scaling ξ_{opt} to maximize the cable efficiency. As the voltage scaling does not consider the produced power, the optimal operation voltage will not be attained at all times. Subsequently the operation current will most likely not be contained within the cable’s rated current limit for all production levels.

3 Design of dynamic model

The dynamic model that is to be created, is based on the simplified system model presented in Fig. 5, but rather than consider the voltage sources to consist of transformers with OLTC, V_1 and V_2 are considered consisting of back-to-back DC converters. The use of back-to-back DC converters enables the AC systems to have different and incompatible parameters for frequency, voltage level or short-circuit power level. It also enables faster regulation of the operation voltage than a transformer with OLTC. The principle of the back-to-back DC is to transform the AC to DC and adjust the voltage and current when the DC is transformed back to AC. The converter consists of a rectifier and an inverter with an energy storage capacitor between them that decouples the operation of the two converters. With a back-to-back DC converter, the rectifier and inverter is placed in the same converter station. A simple block diagram of the converter is presented in Fig. 14. [13], [14], [15]

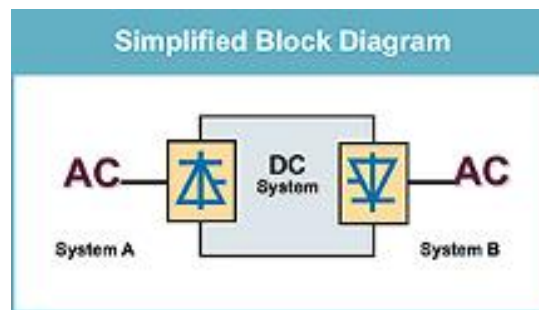


Fig. 14. Back-to-back DC converter. [14]

The system in Fig. 5 consists of three parts; the AC cable and the voltage sources V_1 and V_2 . The thesis will investigate both the use of fixed and variable operation voltage at the grid side (voltage source V_2) for increasing the active power transmission of a 200 km long HVAC cable. There will therefore be made two models of the system. Both models will be constructed the same way, with the exception of the voltage source V_2 .

The method of producing the dynamic system will be presented in this chapter. The details of creating each part of the system will be explained.

3.1 Model of voltage source V_1

The output an OWF is dependent on the wind, which is changing randomly. The OWF's production is therefore dependent on the level of wind present at the moment. The system presented in [1] is not considering the input power from the wind to the OWF, but considers the output active power produced by the OWF. V_1 should be represented as a three-phase voltage source that delivers power based on a power input that refers to the OWF's production level.

As a voltage source by itself in a dynamic simulation in Simulink is unable to produce a controlled power output, a voltage source converter (VSC) with a closed-loop active power control systems has to be designed.

3.1.1 Voltage source converter

The goal of the VSC is to make a control loop, which works on the principle of getting a control value equal to a reference value. In this case, one wants control of the voltage by the input of a power reference. The control loop that is to be designed is presented in Fig. 15. The control loop consists of two PI-regulators one in each of the inner and outer controller. [16]

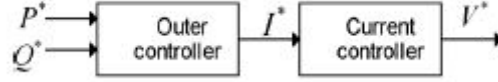


Fig. 15. Voltage source converter, with an outer power controller and an inner current controller. [17]

The control loop in Fig. 15 consists of an outer power controller (OPC) and an inner current controller (ICC). The OPC is given a reference active and reactive power, P^* and Q^* . The inputs to the OPC also include the measured active and reactive power from the VSC. By the PI-regulator in the OPC the difference between the reference values and measured values creates a reference current I^* . This reference value is sent into the ICC and with the input of measured voltages and currents from the VSC, the PI-regulator in the ICC creates the voltage reference V^* . The reference voltage is sent into the voltage source, which then adjusts the output voltage. When the power measurement is equal to the power reference, the controller has reached its goal.

Now a more elaborate description of how the controller was made will be given, which is based on [16], [17] and [18].

3.1.1.1 Inner current controller

The first step of making the ICC is to set up the basic equation of the system, (17).

$$V_{abc} = R \cdot i_{abc} + L \frac{d}{dt} \cdot i_{abc} + V_{abc,conv} \quad (17)$$

V_{abc} are the AC voltages, i_{abc} are the AC currents and $V_{abc,conv}$ are the converter input voltages. R and L are the resistance and the inductance between the VSC and the grid.

To achieve a better performance the control design is made in the dq reference frame. The conversion from abc quantities to dq quantities and opposite is done by the use of Park's transformation, (18) and (19) respectively.

$$\begin{pmatrix} \cos \theta & \sin \theta \\ -\sin \theta & \cos \theta \end{pmatrix} \quad (18)$$

$$\begin{pmatrix} \cos \theta & -\sin \theta \\ \sin \theta & \cos \theta \end{pmatrix} \quad (19)$$

From the Park's transformation, one gets the following equations for d- and q- reference frame, (20) and (21).

$$L \cdot \frac{di_d}{dt} = -R \cdot i_d + \omega L \cdot i_q - V_{d,conv} + V_d \quad (20)$$

$$L \cdot \frac{di_q}{dt} = -R \cdot i_q + \omega L \cdot i_d - V_{q,conv} + V_q \quad (21)$$

To produce a more general control it is necessary to use a p.u. system. The p.u. values are obtained by dividing the nominal values by base values. The base values for the voltage (22), current (23), apparent power (24), angular speed (25), impedance (26) and inductance (27) are calculated from the nominal voltage V_n , current I_n and frequency f_n .

$$V_b = \frac{\sqrt{2}}{\sqrt{3}} \cdot V_n \quad (22)$$

$$I_b = \sqrt{2} \cdot I_n \quad (23)$$

$$S_b = \frac{3}{2} \cdot V_b I_b \quad (24)$$

$$\omega_b = 2\pi f_n \quad (25)$$

$$Z_b = \frac{V_b}{I_b} \quad (26)$$

$$L_b = \frac{V_b}{\omega_b I_b} \quad (27)$$

When all the base values are obtained, equation (20) and (21) are divided by the base voltage V_b to find the p.u. equations for the d- and q-sequence.

$$\frac{L_{pu}}{\omega_b} \cdot \frac{di_{d,pu}}{dt} = -R_{pu} \cdot i_{d,pu} + \omega_{pu} L_{pu} \cdot i_{q,pu} - V_{d,conv,pu} + V_{d,pu} \quad (28)$$

$$\frac{L_{pu}}{\omega_b} \cdot \frac{di_{q,pu}}{dt} = -R_{pu} \cdot i_{q,pu} + \omega_{pu} L_{pu} \cdot i_{d,pu} - V_{q,conv,pu} + V_{q,pu} \quad (29)$$

By cross coupling, $\omega_{pu} L_{pu} i_{q,pu}$ and $\omega_{pu} L_{pu} i_{d,pu}$ can be removed. The d- and q-component dependency from equation (28) and (29) are then removed. Further by neglecting the resistance R_{pu} and model $V_{Conv,pu}$ as a disturbance from (28) and (29), the ICC can be designed as shown in Fig. 16.

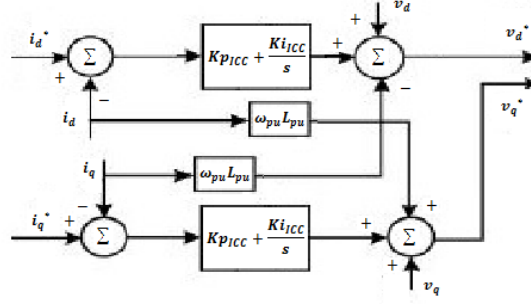


Fig. 16. Inner current controller. [17]

Here i_d^* and i_q^* are the reference currents, i_d , i_q , v_d and v_q are the measured currents and voltages, v_d^* and v_q^* are the reference voltages. $\omega_{pu}L_{pu}$ is the cross coupling with the p.u. values of the angular speed ω and the inductance L . $K_{i_{ICC}}$ and $K_{p_{ICC}}$ are the proportional and integral gain and represents the PI-regulator. The output of the regulator is the sum of the two components. The method used for tuning the regulator and to optimize the ICC is called modulus optimum and work on the principle of removing the dominating time constant. For tuning the PI-regulator the parameters of interest are the gain K_p and the time constant τ_i . The block diagram in Fig. 17 show the simplified block diagram of the ICC.

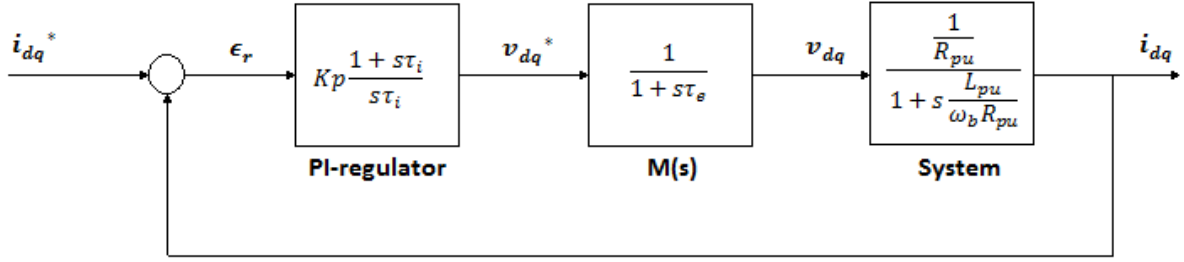


Fig. 17. Simplified block diagram of the inner current controller. [16]

From this, the open loop transfer function of the system can be written as (30).

$$G_{ol,ICC} = Kp \frac{1 + s\tau_i}{s\tau_i} \frac{1}{1 + s\tau_e} \frac{1}{1 + s \frac{L_{pu}}{\omega_b R_{pu}}} \frac{1}{R_{pu}} \quad (30)$$

τ_e is the estimated delay of the pulse modulator (PWM), the analog to digital version conversion, (31).

$$\tau_e = \frac{3}{2} \cdot \frac{1}{f_{sw}} \quad (31)$$

τ_i is equal to K_p divided by k_i and is set so that the dominating time constant is removed, (32).

$$\tau_i = \frac{L_{pu}}{\omega_b R_{pu}} = \frac{Kp}{Ki} \quad (32)$$

By putting (32) into (30), the dominating time constant is canceled and by neglecting the resistance R_{pu} , the closed loop function is found to be (33).

$$G_{cl,ICC} = \frac{G_{ol}}{1 + G_{ol}} = \frac{Kp \frac{1}{\tau_e \tau_i}}{s^2 + s \frac{1}{\tau_e} + \frac{Kp}{\tau_e \tau_i}} \quad (33)$$

(33) is a 2nd order system and can be expressed as (34).

$$s^2 + s \frac{1}{\tau_i} + \frac{Kp}{\tau_e \tau_i} = s^2 + s2\zeta\omega_m + \omega_m^2 \quad (34)$$

From this one can deduce (35) and (36).

$$\omega_m = \frac{1}{2\tau_e \zeta} \quad (35)$$

$$Kp = \frac{\tau_i}{4\tau_e \zeta^2} \quad (36)$$

By inserting (32) into (36) the integral and proportional gain of the ICC becomes (37) and (38).

$$Ki_{ICC} = \frac{1}{4\tau_e \zeta^2} \quad (37)$$

$$Kp_{ICC} = \frac{L_{pu}}{\omega_b R_{pu}} Ki_{ICC} \quad (38)$$

3.1.1.2 Outer power controller

The OWF is only expected to produce active power, the reactive power reference is therefore set to zero. The reactive part of the OPC can then be removed, the controller with only active power control is shown in Fig. 18.

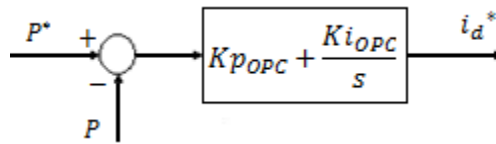


Fig. 18. Outer power controller, with only active power control. [17]

P^* and P are the reference and control value for the active power. i_d^* is the d-component current reference. Kp_{OPC} and Ki_{OPC} are the proportional and integral gain and represents the PI-regulator.

The calculations for tuning the OPC are rather extensive, the tuning is therefore based on an initial guess and further tuning is based on the measuring the alignment of the control value to the reference value. Most often $K_{p_{OPC}}$ and $K_{i_{OPC}}$ are given 1.0 as initial value.

3.2 Model of voltage source V_2

The voltage source on the grid side V_2 should be designed as with both fixed and variable operation voltage. The model for the fixed operation voltage should be represented as a controllable voltage source that can maintain constant voltage independent from the power generated by the OWF.

The model for the variable operation voltage should be able to adjust the voltage depending on the OWF production, but rather than measuring the power from the OWF, the power should be measured at the grid side of the cable to provide a more realistic model. V_2 should therefore be represented as a controllable voltage source dependent on a voltage reference from a control loop with the input of measured instantaneous active power received at the grid side. From the measured power, the voltage reference is given by first calculating the optimal voltage scaling for the given cable length, and then by modifying (15) to (39) the voltage reference is found.

$$V_2 = \sqrt{-\frac{P_{grid}}{\sqrt{3}Re\{(B\xi + A)^*\}}} \quad (39)$$

3.3 Model of HVAC cable

The cable in [1] is an exact PI-equivalent cable, divided into segments to take into account the distributed parameter effects and thereby the variation of voltage and current along the cable. The cable selected should ideally follow the same cable model and thereby also the admittance matrix (7). As the goal of the thesis is to investigate the transmission efficiency of the cable, the segmentation of the cable is not crucial for the cable model and finding an exact PI-equivalent cable model should be prioritized.

4 Simulink model of dynamic system

The development of the dynamic models for fixed and variable operation voltage was done in MathWorks's Simulink. Simulink allows one to model, simulate and analyze a multi-domain dynamic system. A system can be modeled in Simulink as a detailed block diagram by predefined and customizable blocks. Matlab scripts and functions can also be incorporated into the model. [19]

The finalized overall Simulink model for both the models is presented in Fig. 19. All of the components in the model will be further explained in this chapter.

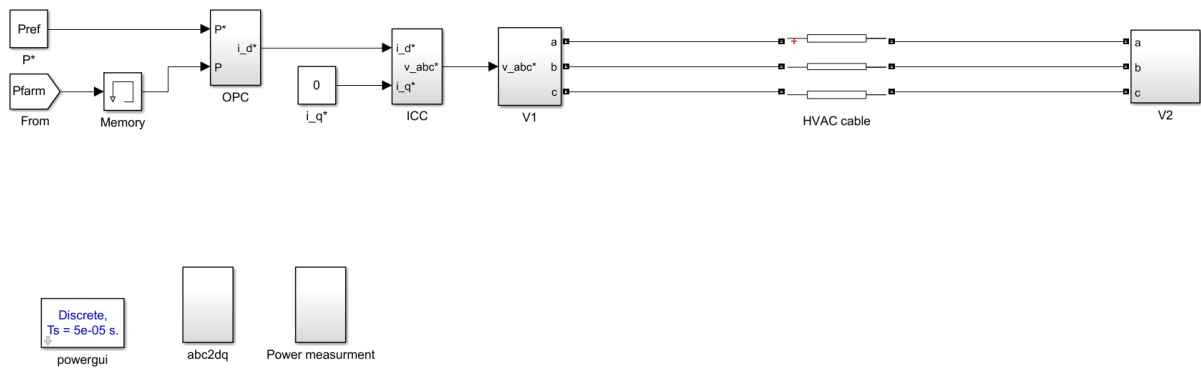


Fig. 19. Model of the HVAC system developed in Simulink.

4.1 Design of voltage source V_1

The model of the voltage source V_1 made in Simulink is presented in Fig. 20. The system is a three-phase system, V_1 should therefore be represented by a three-phase controllable voltage source, where the signal controlling the voltage source is coming from a VSC. As there are no three-phase controllable voltage source in Simulink, it was modeled as three separate controllable voltage sources, with signal from the voltage reference v_{abc}^* from the VSC. The voltage sources are all connected by an inductance to a three-phase VI measurement block, and then to each of their respective output-ports. The inductances are necessary to be able to measure the voltages and currents. The measured voltage V_{abc} and current I_{abc} are both sent to each of their output ports, $v1_{abc}$ and $i1_{abc}$. The angular speed ω multiplied with the time t is measured by the three-phase phase locked loop block, and sent to the output wt . This is used further for the conversion between abc- and dq-reference frame, for the voltages and currents.

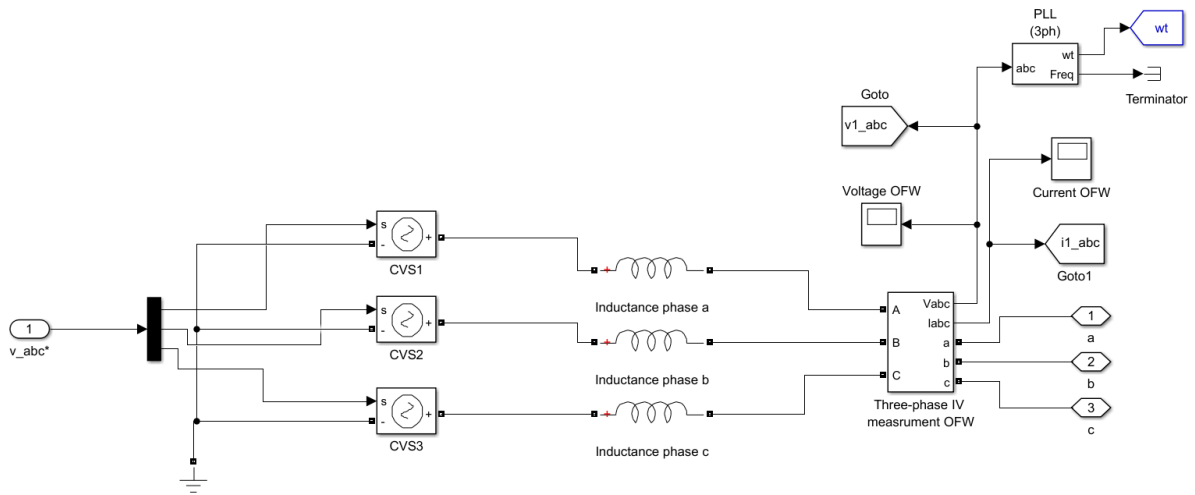


Fig. 20. Simulink model of voltage source V1.

4.1.1 Design of voltage source converter

The VSC is made based on theory presented in chapter 3.1.1.

4.1.1.1 Design of Inner current controller

The ICC was designed first, the Simulink model of the ICC is presented in Fig. 21. $\omega_{pu}L_{pu}$, $K_{p_{ICC}}$ and $K_{i_{ICC}}$ were represented as gains, $w_{pu} * L_{pu}$, $K_{i_{ICC}}$ and $K_{p_{ICC}}$. The inputs are the measured voltages and currents from V₁, the current reference from the OPC, and a zero signal from the constant block i_q^* in Fig. 19. The current references are given as i_d^* and i_q^* and the measured currents and voltages are given as i_d , i_q , v_d and v_q .

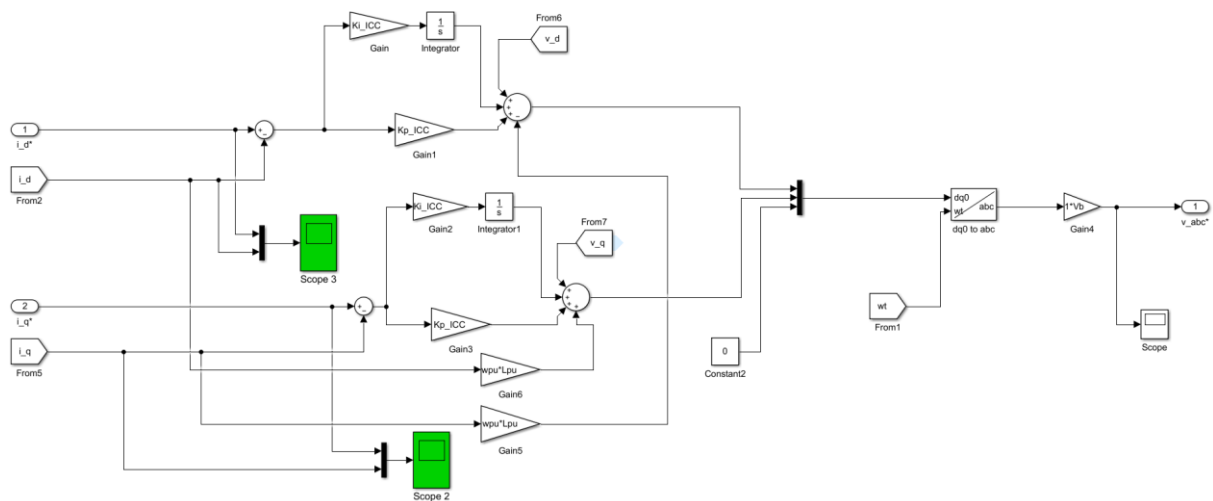


Fig. 21. Simulink model of the inner current controller.

The currents and voltages i_d , i_q , v_d and v_q are found by converting the measured current and voltage $i1_abc$ and $v1_abc$ from the three-phase VI measurement from V₁, Fig. 20.

The abc- to dq-reference frame conversion is done by the abc2dq block in Fig. 19, the detailed model is presented in Fig. 22.

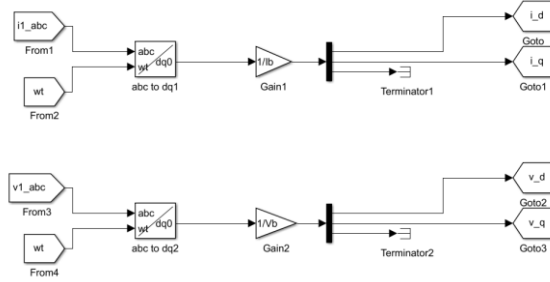


Fig. 22. abc to dq0 conversion of current and voltage.

The abc measured current and voltage are sent into each their separate abc to dq0 transformation block together with the angular speed, the output of the block is a collected dq0 signal which is split by a demux block into separate signals. The zero signal is terminated and the d and q currents and voltages are sent to the ICC. The transformation by the abc to dq0 transformation block is based on (40).

$$\begin{bmatrix} \sin(\omega t) & \sin\left(\omega t - \frac{2\pi}{3}\right) & \sin\left(\omega t + \frac{2\pi}{3}\right) \\ \cos(\omega t) & \cos\left(\omega t - \frac{2\pi}{3}\right) & \cos\left(\omega t + \frac{2\pi}{3}\right) \\ \frac{1}{2} & \frac{1}{2} & \frac{1}{2} \end{bmatrix} \quad (40)$$

The outputs of the ICC (Fig. 21) is the voltage reference v_abc^* , which is converted from dq- to abc-reference frame. Then the signal is multiplied with the base voltage by the gain1*Vb to transform the p.u. value to a real value, which is then sent into the controlled voltage sources of V_1 (Fig. 20), which then adjusts the power. The conversion is done by the dq0 to abc transformation block, were the zero signal is given by a constant block. The transformation is done by equation (41).

$$\begin{bmatrix} \sin(\omega t) & \cos(\omega t) & 1 \\ \sin\left(\omega t - \frac{2\pi}{3}\right) & \cos\left(\omega t - \frac{2\pi}{3}\right) & 1 \\ \sin\left(\omega t + \frac{2\pi}{3}\right) & \cos\left(\omega t + \frac{2\pi}{3}\right) & 1 \end{bmatrix} \quad (41)$$

4.1.1.2 Design of outer power controller

The Simulink model of the OPC is presented in Fig. 23. The OPC consists of two gains, K_{pOPC} and K_{iOPC} . The inputs are the reference active power and the measured active power from V_1 , P^* and P respectively. The controller is able to work in p.u. by dividing the measured active power by the base apparent power S_b , represented by the gain $1/S_b$. The output of the OPC is the current reference i_{d^*} .

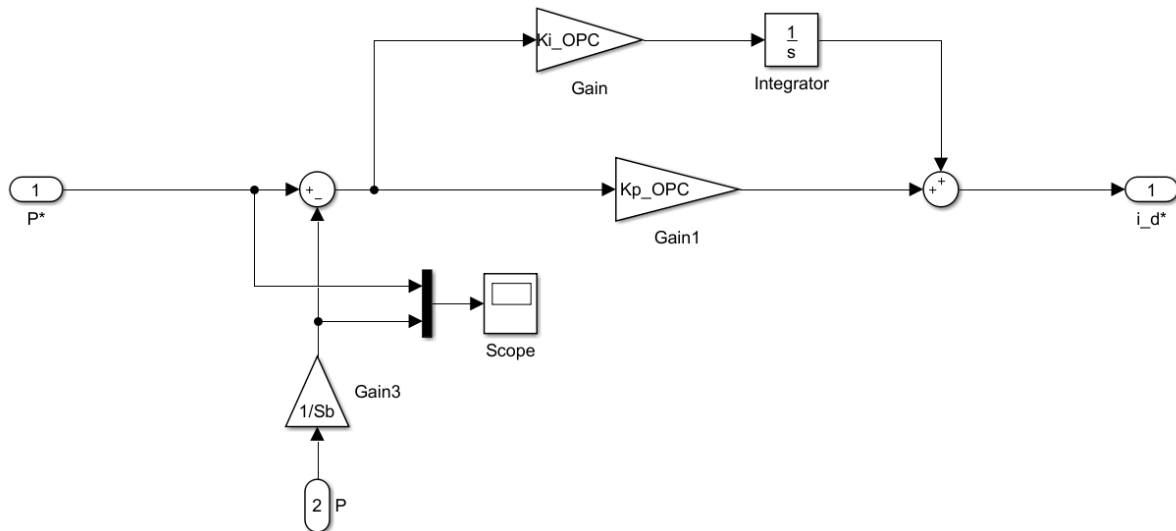


Fig. 23. Simulink model of outer power controller.

The measured active power comes from the output P_{farm} , as shown in Fig. 19. The memory block between the output P_{farm} and input P of the OPC is there to ensure that the OPC has an initial input value so that the simulation is able to start.

4.1.1.3 Tuning of the voltage source converter

To tune the VSC, the script *initiate_200km_cable_sim* was made (appendix A5). The ICC was first tuned. The script first calculated the base values by using (22), (23), (24), (25), (26) and (27). Then the p.u. values were found by dividing the nominal values by the base values. The calculated p.u. values for the tuning the ICC is presented in TABLE V.

TABLE V. Calculated p.u. values from script (appendix A5).

ω_{pu}	1
L_{pu}	0.1931
R_{pu}	0.0797

Further, the damping was selected to be $\frac{1}{\sqrt{2}}$ and the switching frequency was chosen to be 2000Hz. [16] From this, K_{iICC} and K_{pICC} were calculated by (37) and (38). The calculated values are presented in TABLE VI.

TABLE VI. Calculated K_{iICC} and K_{pICC} from script (appendix A5).

K_{iICC}	666.6667
K_{pICC}	5.1389

The tuning of the ICC was tested by comparing the reference and control currents by using the scope shown in Fig. 21. If the control value was following the reference value and would align with it to a satisfactory degree, the tuning was considered correct.

The tuning was first tested for constant values, the inputs ports of the ICC i_d^* and i_q^* was given each a constant value, 1.0 and zero respectively. The control value aligned well with the reference value for i_d . For i_q the control value would not fully align with the reference value. This is most likely a result of the capacitance of the cable is not taken into consideration when tuning the ICC.

The ICC was further tested for varying reference currents, with initial value of 0.3 p.u. and 1.0 p.u. for the final value. The result was that the control value for both i_d and i_q followed the reference value, but would not align completely. The tuning was then tested by only varying the i_d reference value and keeping the i_q reference constant at zero. The result was that the control value for i_d would align with the reference value. The control value for i_q would not fully align with the reference value, and would jump and move further from the reference value when the i_d reference would increase. This further highlight that the tuning does not consider the cable capacitance. The tuning of the ICC is however considered to be at a satisfactory level (the results of the tuning tests are shown in appendix B1).

The tuning of the OPC was done by an initial guess and from that the scope in Fig. 23 was used to find the values that corresponded with the control value aligning with the reference value. K_{pOPC} and K_{iOPC} were first given an initial value of 1.0. Simulink would not simulate with these values. Both of the gains were then set to $1.0e-3$, Simulink was then able to simulate the system. The control value was however not following the reference value, the control value was found to be equal to zero for the entire simulation as shown in Fig. 24.

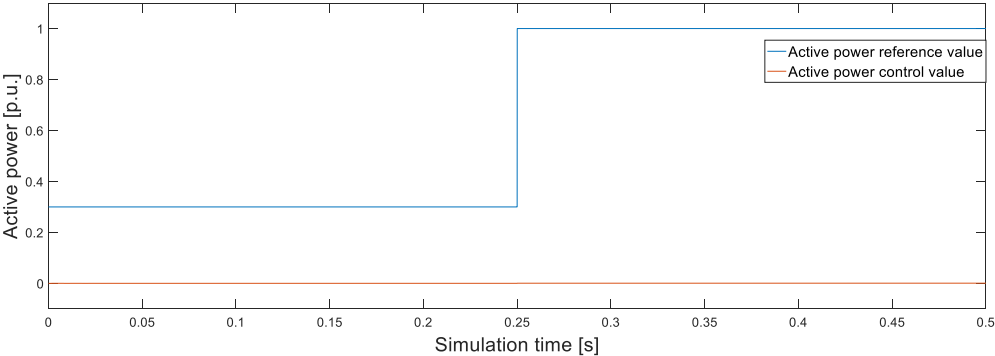


Fig. 24. Incorrect tuning of the outer power controller.

When trying to change the gain values, K_{pOPC} was found to be unable to change, as the simulation would then be unable to run. As the relationship between the control and reference value should be 1 to 1 ratio, K_{iOPC} was set to 1000 to equalize the difference. The result was that the control value followed the reference value, as shown in Fig. 25.

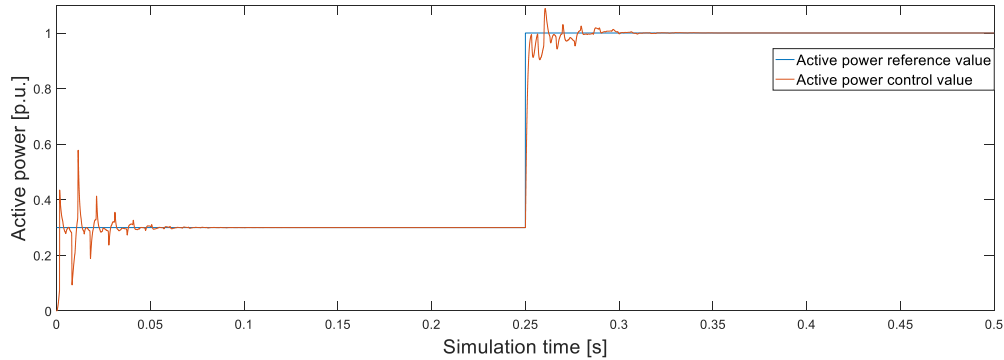


Fig. 25. Correct tuning of the outer power controller.

The controller was now working, however there were some fluctuation before the control value aligned with the reference value when the simulation starts or when the reference value is changing at 0.25s. The stabilization time is approximately 0.07s.

4.2 HVAC cable selection

The cable model that was selected is a distributed parameters line. It was selected on the bases that it was the only cable that did not lead to the power from the voltage sources V_1 and V_2 to oscillate terrible. The cable is however not an exact PI equivalent cable as presented in [1], this will most likely result in problems for the model of variable operation voltage.

4.3 Design of voltage source V_2

There are two models for the voltage source V_2 , fixed operation voltage model and variable operation voltage model. Both models have the same construction for the voltage and current measurement and voltage sources. There are three input ports that are connected to a three-phase VI measurement block and then to three separate controllable voltage sources. The measurement of current and voltage by the three-phase measurement block is sent to each there output-port, $i2_abc$ and $v2_abc$, as shown in Fig. 26 and Fig. 27. The difference between the two models is that for the fixed operation voltage model the signal to the controllable voltage sources is a constant sine wave function where each sine wave function is given an amplitude value and phase angle, as shown in Fig. 26.

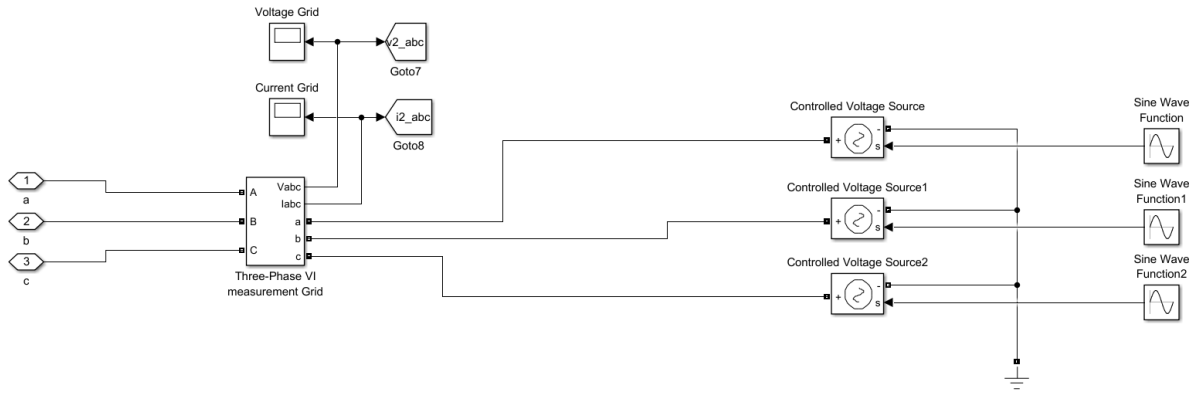


Fig. 26. Simulink model of the voltage source V_2 with fixed operation voltage.

The Simulink model of the voltage source V_2 with variable operation voltage is presented in Fig. 27. The voltage source V_2 regulates the voltage by a control loop where the measured active power at the grid side of the cable P_{grid} , is sent into a Matlab function where the variable operation voltage is calculated. The Matlab function (appendix A6) calculates the voltage scaling for the given cable length and calculates the optimal operation voltage from the measured power received at the grid side, by using (39). The output value of the function is split into three parts. One for each phase, v_{2a} , v_{2b} and v_{2c} . Then each of voltages are multiplied with a sine wave function where the amplitude is set to 1.0 and the respective phase angle is given. The signals are then sent into each their controllable voltage sources through a memory block from va_2 , vb_2 and vc_2 . The memory block is there to give an initial value for the simulation to be able to run.

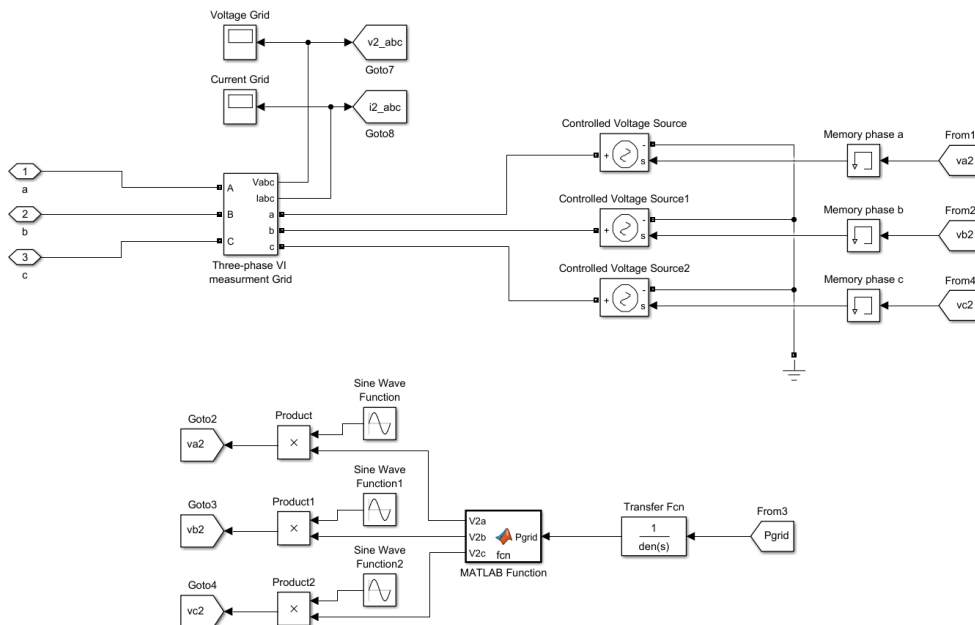


Fig. 27. Simulink model of the voltage source V_2 with variable operation voltage.

From this control loop the voltage sources regulate the voltage to the instantaneous power received at the grid side. The transfer function in the control loop is a filter, which ensures that the power signal is smooth and does not fluctuate too badly.

4.4 Power Measurement

The active and reactive power measurement from the voltage sources V_1 and V_2 is done by the power measurement block in Fig. 19. The Simulink model of the power measurement block is presented in Fig. 28. The input values to the block is the measured voltages and currents from V_1 and V_2 , $v1_abc$, $v2_abc$, $i1_abc$ and $i2_abc$. The inputs are put into the power (3ph, instantaneous) block, which calculates the active and reactive power. The active power for both V_1 and V_2 is sent to output Pfarm and Pgrid respectively. The active and reactive power from V_1 and to V_2 is measured by each their individual scope, which saves the data of each simulation.

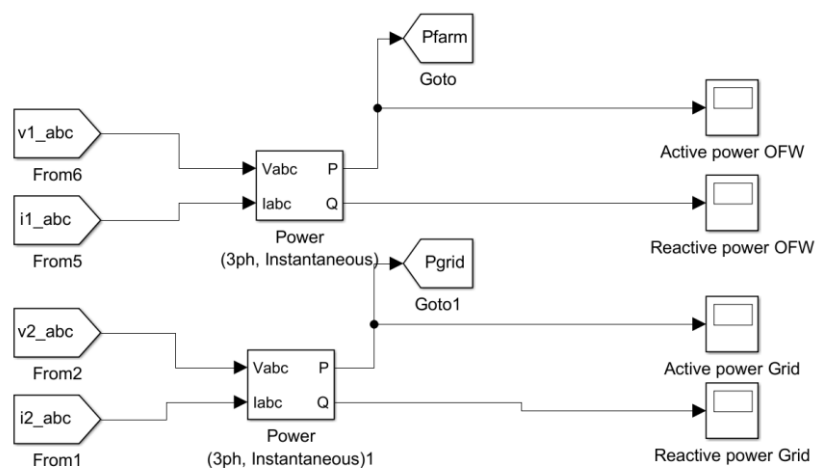


Fig. 28. Simulink model of the power measurement block shown in Fig. 19.

4.5 Powergui

The powergui block is necessary when simulating Simscape power systems. The block allows one to choose from the methods continuous, discretization or phasor solution to solve the model simulation. The method chosen for simulating the models was discretization, which allows the use of fixed time step for the simulation. The time step that was chosen was $50e-6$, which was necessary for the variable operation voltage model simulation to be able to work.

5 Results

The dynamic models made for fixed and variable operation voltage for the voltage source V_2 were to be simulated for minimum to maximum production from voltage source V_1 . The maximum production 1.0 p.u. power, should be the same as in [1], 320 MW.

To simulate the fixed operation voltage model, the input values are the p.u. voltage for the voltage source V_2 and the p.u. power production from the voltage source V_1 . The variable voltage model was only given input for the power production from the voltage source V_1 . The models were simulated for 0.5s. The results of the simulations are the measured active power from the voltage sources V_1 and V_2 , and the measured current and voltage at the voltage source V_2 .

The system performance is assessed by the result of the calculated cable efficiencies, which is found by using (8) for the average measured active power at both ends of the cable. The average measured active power is calculated from the point the power has stabilized. The measured currents and voltages are considered for the viability of the system, investigating if the cable is operating within its limits.

5.1 Active power production test simulation

Both the models were first simulated for 1.0 p.u. production to investigate the active power production by the voltage source V_1 , and to find the stabilization time for the measured active power at each end of the cable. The operation voltage of the voltage source V_2 for the variable operation voltage model was also measured to find the stabilization time. The fixed voltage model simulation was given 1.0 p.u. voltage for voltage source V_2 .

The result for the active power sent from the voltage source V_1 for the fixed and variable operation voltage model simulations, are presented in Fig. 29 and Fig. 30. The result for the active power received at the voltage source V_2 for the fixed and variable operation voltage model simulations are presented in Fig. 31 and Fig. 32. The measured operation voltage at voltage source V_2 for the variable operation voltage model simulation is presented in Fig. 33.

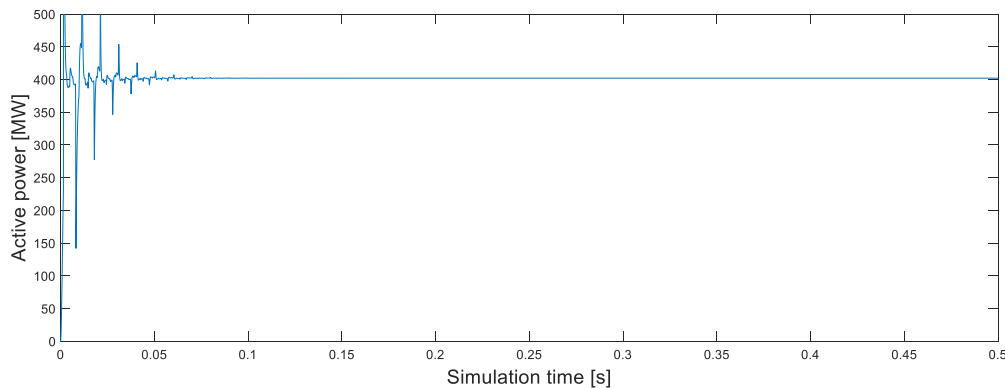


Fig. 29. 1.0 p.u. active power production from V_1 . With 1.0 p.u. fixed operation voltage at V_2 .

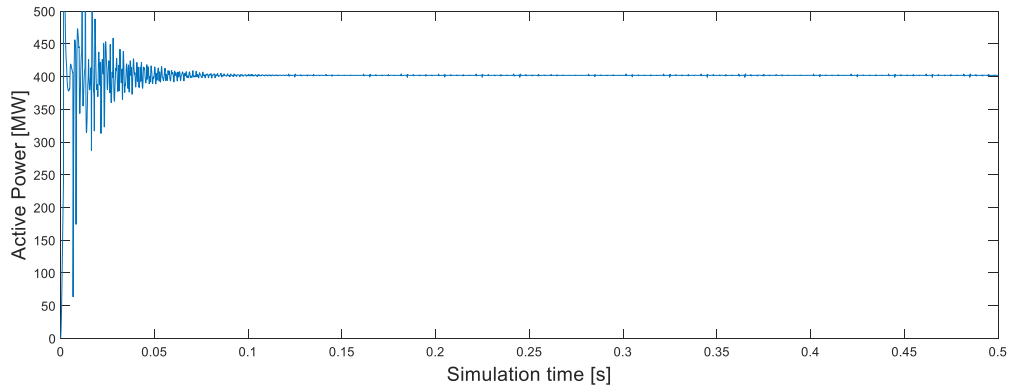


Fig. 30. 1.0 p.u. active power production from V₁. With variable operation voltage at V₂.

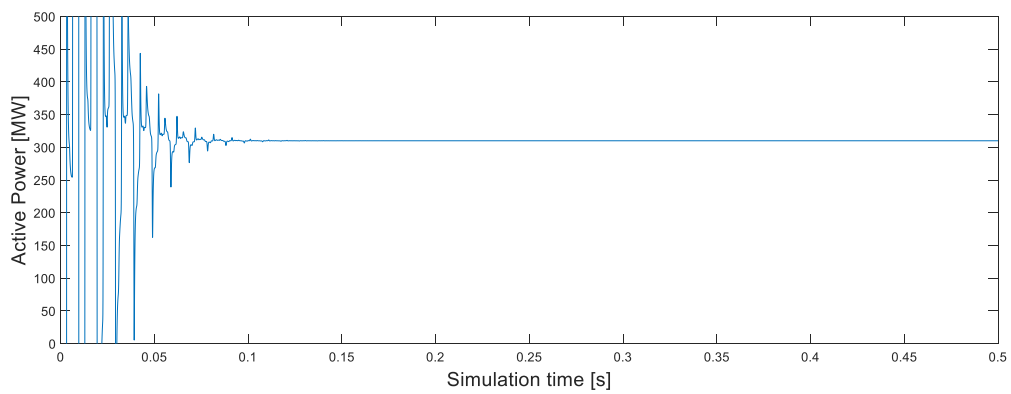


Fig. 31. Active power received at grid for 1.0 p.u. production by V₁. With 1.0 p.u. fixed operation voltage at V₂.

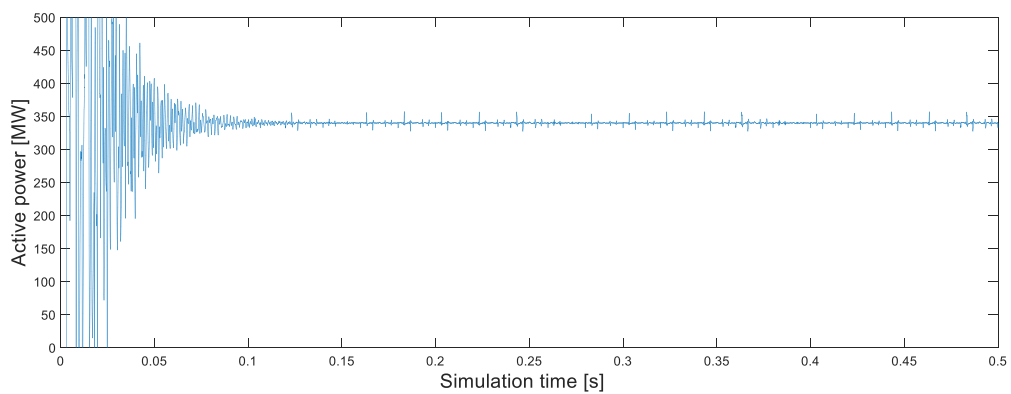


Fig. 32. Active power received at grid for 1.0 p.u. production by V₁. With variable operation voltage at V₂.

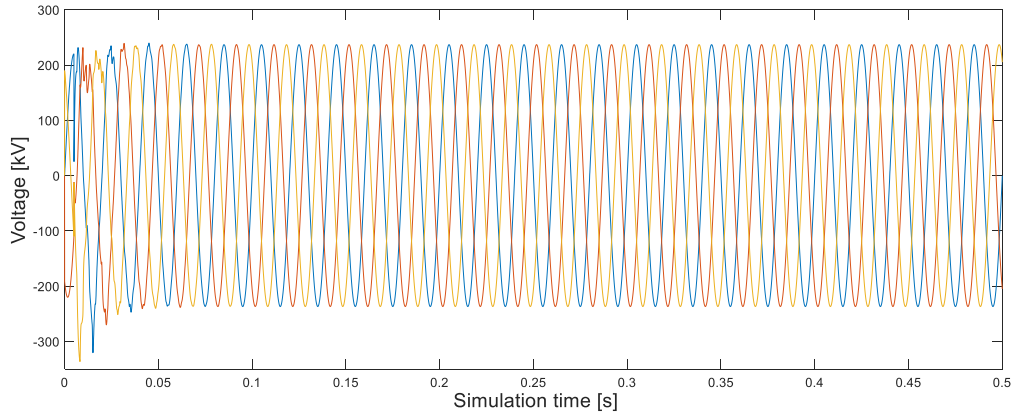


Fig. 33. Operation voltage of voltage source V_2 with variable operation voltage for 1.0 p.u. production by V_1 .

From the simulations, the power production by the voltage source V_1 for both simulations was found to be higher than in [1], Fig. 29 and Fig. 30. The active power is found to be 402 MW, when it has stabilized after approximately 0.07s. V_1 in [1] for 1.0 p.u. production is equal to 320 MW. The p.u. values for power production is not found to be the same. To avoid that the simulations consider power production levels that exceed the maximum level of the system presented in [1], the maximum p.u. production is adjusted for the further simulation. The maximum power production used further in this thesis will therefore be 0.8 p.u., which is equal to 321.6 MW.

Fig. 30 shows that when the power stabilizes for the variable operation voltage model simulation, the power will oscillate more compared to the fixed operation voltage model simulation, Fig. 29. This comes from the control loop that regulates the voltage for the voltage source V_2 to the active power received at grid side of the cable. The same difference in oscillation can be seen between the fixed and variable operation voltage model simulations for the receiving active power for voltage source V_2 , Fig. 31 and Fig. 32. The receiving active power at voltage source V_2 (Fig. 32) is seen to oscillate more compared to the sent active power from voltage source V_1 (Fig. 30).

Still this will not affect the results of the calculation of the cable efficiency, as it only considers the average active power when the power has stabilized (>0.07 s). The oscillations should neutralize each other when calculating the average value of the active power.

The variable operation voltage measured at voltage source V_2 is found to have approximately the same stabilization time as the active power, Fig. 33. The operation voltage stabilizes at 0.762 p.u. voltage; this is lower than expected.

5.2 Cable efficiency

Both the models were simulated for variation of 0.1 to 0.8 p.u. power production by the voltage source V_1 , based on the test simulations. The fixed operation voltage model was simulated from 0.1 to 1.0 p.u. voltage at the voltage source V_2 . The stabilization time selected for the calculation of the average active power at both ends was 0.1s.

The result of the calculated cable efficiency from the simulations of fixed and variable operation voltage is presented separately in Fig. 34 and Fig. 35. The figures do not however consider the negative cable efficiencies, all the calculated cable efficiencies are presented in appendix B2. The points are either represented as * or ·, which denotes if the operation current of the cable is within or exceeding the cable’s current limit, respectively.

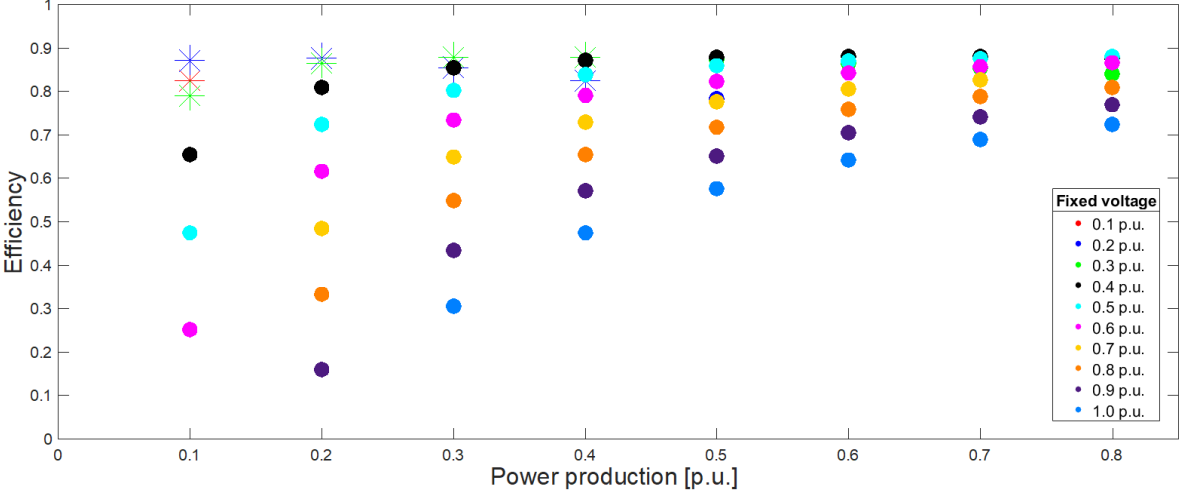


Fig. 34. Calculated cable efficiencies for all the fixed operation voltage model simulations, within the efficiency area zero to 1. * and · denote that the operation current is within or exceeds the cable’s current limit, respectively.

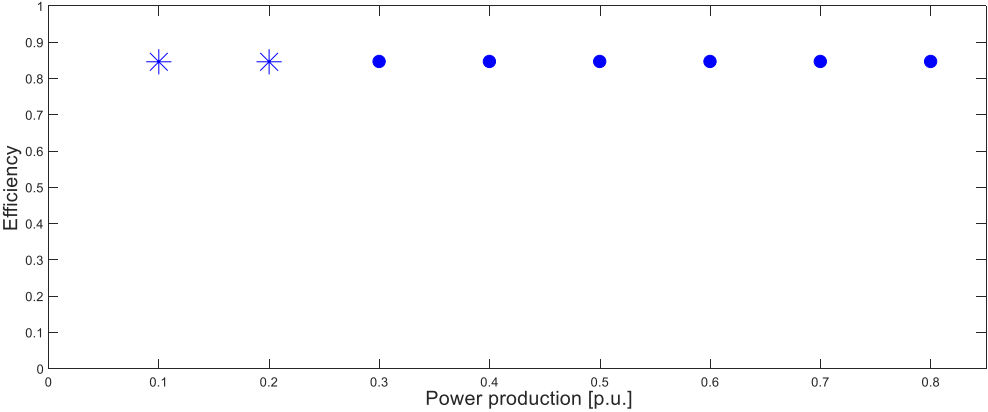


Fig. 35. Calculated cable efficiency for the variable operation voltage model simulation, within the efficiency area zero to 1. * and · denote that the operation current is within or exceeds the cable’s current limit, respectively.

The highest efficiency is found in Fig. 34 (appendix B2), 0.880 and is found for 0.4 p.u. fixed operation voltage for 0.6 p.u. production. From Fig. 34 and Fig. 35, the variable operation voltage model, the 0.3, 0.4, 0.5 and 0.6 p.u. fixed operation voltage model simulations are the only ones that have a positive calculated efficiency for each production level. The 0.1 and 0.2 p.u. fixed operation voltage model simulations have not any points for higher production scenarios. The 0.7, 0.8, 0.9 and 1.0 p.u. fixed operation voltage model simulations have some missing points for low production levels. The missing points mean that the calculated efficiency is negative, the voltage source V_2 is then sending active power in the direction of the cable to

compensate for the cable losses. The calculated cable efficiencies for the variable operation voltage model (Fig. 35) is found to be constant for all the production levels, 0.846.

Most of the simulations are found to have operation current that exceeds the cable’s current limit. The simulations that maintain the operation current within the cable limit is the variable voltage model, the 0.1, 0.2 and 0.3 p.u. fixed voltage models for low production levels.

By looking closer at the simulations of 0.2 and 0.3 p.u. fixed operation voltage simulations, Fig. 36 and Fig. 37, it is shown that the cable efficiency will decline when the production increases for low voltage levels. This is best illustrated in Fig. 36, for 0.2 p.u. fixed operation voltage.

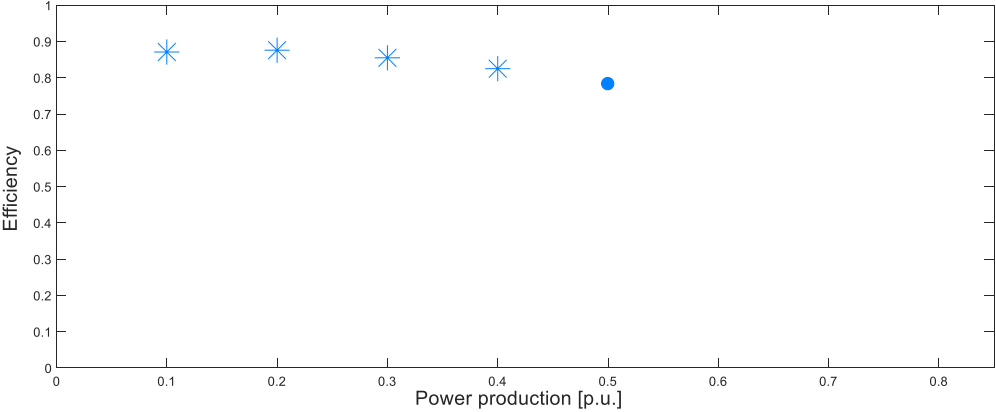


Fig. 36. Cable efficiency as a function of p.u. power production by V_1 for 0.2 p.u. fixed operation voltage at V_2 , within the efficiency area zero to 1. * and · denote that the operation current is within or exceeds the cable’s current limit, respectively.

The 0.2 p.u. fixed operation voltage model has no points from 0.6 to 0.8 p.u. power production. The operation current is kept within the cable limit from 0.1 to 0.4 p.u. power production.

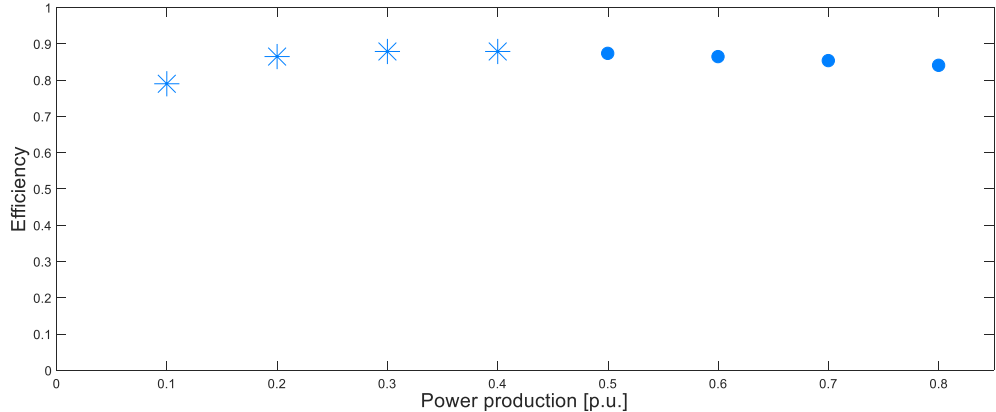


Fig. 37. Cable efficiency as a function of p.u. power production by V_1 for 0.3 p.u. fixed operation voltage at V_2 , within the efficiency area zero to 1. * and · denote that the operation current is within or exceeds the cable’s current limit, respectively.

Fig. 37 shows that the cable efficiency increases from 0.1 to 0.3 p.u. production. From 0.4 p.u. production, the cable efficiency declines and the operation current is not within the cable’s current limit.

Fig. 38 and Fig. 39 show 0.9 and 1.0 p.u. fixed operation voltage respectively. The operation current is not kept within the cable’s current limit at any of the production levels.

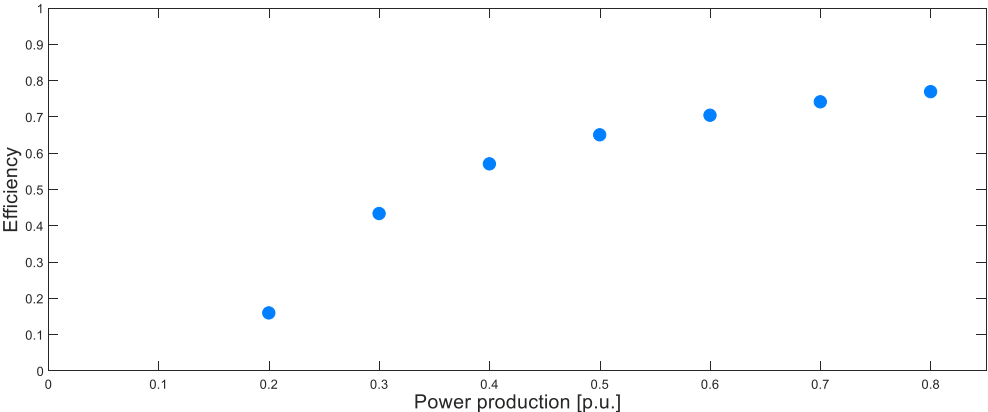


Fig. 38. Cable efficiency as a function of p.u. power production by V_1 for 0.9 p.u. fixed operation voltage at V_2 , within the efficiency area zero to 1. * and · denote that the operation current is within or exceeds the cable’s current limit, respectively.

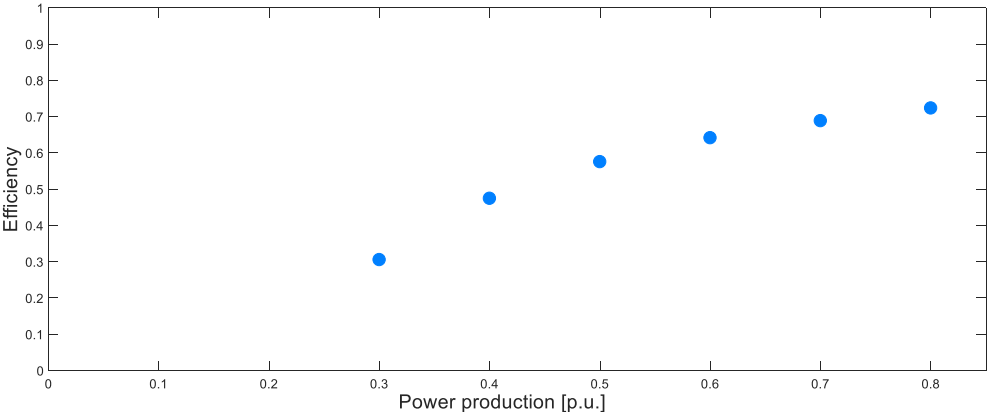


Fig. 39. Cable efficiency as a function of p.u. power production by V_1 for 1.0 p.u. fixed operation voltage at V_2 , within the efficiency area zero to 1. * and · denote that the operation current is within or exceeds the cable’s current limit, respectively.

There are missing points at low production for the 0.9 and 1.0 p.u. fixed voltage model simulations, Fig. 38 and Fig. 39. The cable efficiency for both the simulations is shown to increase when the production increases.

The cable efficiency of the variable operation voltage simulations is found to be the same for all production levels, Fig. 37. Therefore, it is more interesting to see the p.u. voltage of V_2 as a function of the power production, the result is illustrated in Fig. 40.

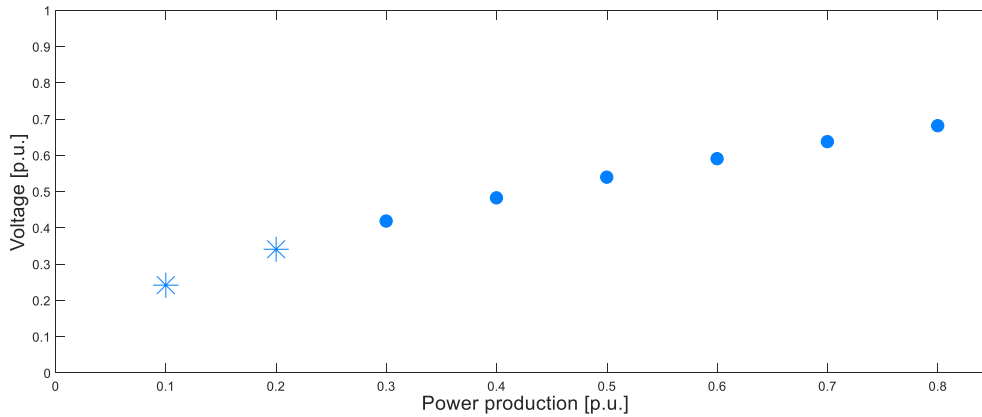


Fig. 40. Operation voltage as a function of p.u. power production by V_1 for variable operation voltage at V_2 , within the efficiency area zero to 1. * and · denote that the operation current is within or exceeds the cable's current limit, respectively.

The voltage is seen to increase when the power production is increasing. The voltage varies from 0.242 to 0.681 p.u. voltage (appendix B2). The current is only maintained within the cable limit for 0.1 and 0.2 p.u. production.

5.3 Summation of results

Fig. 34 shows that there are a lot of missing points for the fixed operation voltage model simulations, this is a result of some of the cable efficiencies are found to be negative. A negative cable efficiency represent that V_2 is sending active power to compensate for the cable losses. The negative efficiencies are found at high production levels for low operation voltage and at low production levels for high operation voltage. Both scenarios result in high charging currents.

Almost all of the simulations have operation current, which exceeds the current limit of the cable. If the current limit of the cable is disregarded, Fig. 36, Fig. 37, Fig. 38 and Fig. 39 show that operation voltage affects the cable efficiency. At low operation voltage, the cable efficiency decreases when the production increases. For high operation voltage, the cable efficiency increases when the production increases. The simulations for lower operation voltage are found to have the highest cable efficiency. The result from the simulation of the variable operation voltage model presented in Fig. 40, show that by increasing the voltage to the increase of produced power the cable efficiency will be kept constant. The variation in operation voltage for changes in power production is small, varying from 0.242 to 0.681 p.u. voltage.

The simulations that are able to maintain the operation current within the limit at some production levels are the variable operation voltage model and the fixed operation voltage model for 0.1, 0.2 and 0.3 p.u. voltage. The variable operation voltage model is able to maintain the operation current to 0.2 p.u. production, 80.4 MW. The 0.1 p.u. fixed operation voltage model maintain the operation current to 0.1 p.u. production, 40.2 MW. The 0.2 and 0.3 p.u. fixed operation voltage model maintain the operation current to 0.4 p.u. production, 160.8 MW. The fixed operation voltage model for 0.2 and 0.3 p.u. voltage are found to have the highest average cable efficiency and largest operation area for the power production.

The variable operation voltage model should be able to attain the highest cable efficiency at all production levels, and still maintain the operation current within the cable's limit. The results of the simulations contradict this statement. Ideally, the simulations for high operation voltage for high power production would attain the highest cable efficiency, as those scenarios have the highest gain.

There are found dissimilarities when comparing the simulated results for the fixed operation voltage model with the results from [1]. None of the simulations for the fixed operation voltage model are found to have as high cable efficiency as in [1]. The results of the simulations for the low fixed operation voltages (0.2 and 0.3 p.u. voltage) are found to have a higher operation area for the produced power. The results of the simulations for high fixed operation voltages (0.9 and 1.0 p.u. voltage) are found to have a higher demand of produced power to transmit power. The charging currents are also observed to increase more for the increase in power production compared to [1]. The same can be observed for the increase of operation voltage.

The same are observed for the variable operation voltage model. Fig. 8 from [1] show that the operation voltage is the first to exceed the limit of the cable at 170 MW power production, the operation current is not exceeded before the power production is 250 MW. The reason explaining the dissimilarities between the results of [1] and the simulations of the variable operation voltage model may be the voltage scaling. The voltage scaling is put to a fixed value, based on the cable parameters and the cable length. It does not adjust to the instantaneous power received at the grid side of the cable. This enables the operation current of the variable operation voltage model to exceed the current limit of the cable. Still if the voltage scaling is calculated correctly, the highest attainable efficiency should be found.

The high demand for transmission and the higher charging currents suggests that the cable used in the simulations is not following the same cable model as the one used in [1].

6 Conclusion

Comparing the simulations for fixed and variable operation voltage done in this thesis, the fixed operation voltage model for low voltage (0.2 and 0.3 p.u.) was found to be the best option. As it has the highest average efficiency and the largest operation area without exceeding the current limit of the cable.

The results of the simulations contradict the findings presented in [1], which state that by regulating the operation voltage to the power production one should attain the highest cable efficiency. As the voltage scaling for the variable operation voltage model is not continuously adjusted to the instantaneous active power, the model will be unable to maintain the operation current within the current limit of the cable.

the optimal voltage level will not be found at all times. This affects the variable operation voltage model's capability to maintain the operation current within the current limit of the cable.

However, comparing the result of the simulations in [1], the charging currents are observed to increase more for higher operation voltage or produced power. This suggest that the cable selected is not using the same cable model as the one used in [1]. The cable seems to have a higher capacitive characteristic, which then demands a higher compensation. The result is that the voltage scaling will be incorrect, as it is calculated for a different cable model. The maximum attainable cable efficiency of the cable is therefore less than in [1].

The use of controlling the voltage is however shown to work. As with low operation voltages for low production the cable efficiency is high and likewise for high operation voltages for high production. The result also shows that when using a fixed operation voltage a low operation voltage should be selected, as the average cable efficiency for variation in production will be higher.

Further work should be to either produce a cable in Simulink, which is equal to the one used in [1], or calculate the voltage scaling to the cable used in the thesis. Further one should develop a Matlab function or a controller for the voltage source V_2 , which calculates the voltage scaling for the instantaneous active power, so that the maximum attainable cable efficiency is found within the limits of the cable's operation area. From this model one can further investigate a more realistic power production by the voltage source V_1 that is based on a typical wind profile, to see what the actual gain of using variable operation voltage compared to fixed operation voltage.

7 Bibliography

- [1] B. Gustavsen and O. Mo, "Variable Transmission Voltage for Loss Minimization in Long Offshore Wind Farm AC Export Cables," *IEEE Transactions on Power Delivery*, 2016.
- [2] G. M. Masters, *Renewable And Efficient Electric Power Systems*, New Jersey: John Wiley & Sons, Inc, 2013, pp. 475-477.
- [3] S. Lauria, M. Schembari and F. Palone, "EHV AC Interconnection for a GW-size Offshore Wind-Farm Cluster: Preliminary Sizing," *Energy Conference (ENERGYCON)*, 2014 IEEE International, 2014.
- [4] P. Kundur, *Power System Stability and Control*, (India) Edition ed., New York: McGraw Hill Education, 2014, pp. 199-231, 627-652.
- [5] "electrical4u," [Online]. Available: <https://www.electrical4u.com/ferranti-effect-in-power-system/>. [Accessed 24 May 2017].
- [6] S. Kolluri, P. Thummala, R. Sapkota, S. K. Panda and D. Rendusara, "Subsea Power Transmission Cable Modelling: Reactive Power Compensation and Transient Response Studies," *IEEE*, 2016.
- [7] J. Ruddy, R. Meere and T. O'Donnell, "Low Frequency AC transmission as an alternative to VSC-HVDC for grid interconnection of offshore wind," in *PowerTech, 2015 IEEE Eindhoven*, Eindhoven, Netherlands, 2015.
- [8] G. Guidi and O. B. Fosso, "Investment Cost of HVAC Cable Reactive Power Compensation Off-shore," *Energy Conference and Exhibition (ENERGYCON)*, 2012 IEEE International, 2012.
- [9] Z. Guiping, D. Xiaowei and Z. Chen, "Optimisation of reactive power compensation of HVAC cable in off-shore wind power plant," *IET Renewable Power Generation*, 2015.
- [10] H. Brakelmann, "Loss determination for long three-phase high-voltage submarine cables," *ETEP*, vol. 13, no. 3, pp. 193-197, May/June 2003.
- [11] "Wikipedia," [Online]. Available: https://en.wikipedia.org/wiki/Characteristic_impedance. [Accessed 23 May 2017].
- [12] "Microwaves101," [Online]. Available: <https://www.microwaves101.com/encyclopedias/propagation-constant>. [Accessed 23 May 2017].
- [13] N. Mohan, T. M. Undeland and W. P. Robbins, *Power Electronics*, John Wiley & Sons, Inc., 2013, p. 10.

- [14] "Siemens," [Online]. Available: <http://www.energy.siemens.com/us/en/power-transmission/hvdc/applications-benefits/configurations/back-to-back-hvdc.htm>. [Accessed 9 March 2017].
- [15] "GE Grid Solutions," [Online]. Available: <https://www.gegridsolutions.com/AlstomEnergy/grid/products-services/product-catalogue/electrical-grid-new/hvdc/hvdc-solutions/hvdc-back-to-back/>. [Accessed 23 May 2017].
- [16] C. Bajracharya, M. Molinas, J. A. Suul and T. M. Undeland, "Understanding of tuning techniques of converter controllers for VSC-HVDC," 9-11 June 2008.
- [17] W. Wang, A. Beddard, M. Barnes and O. Marjanovic, "Analysis of Active Power Control for VSC–HVDC," in *IEEE Power & Energy Society*, 2014.
- [18] J. Beerten, S. D'Arco and J. A. Suul, "Identification and small-signal analysis of interaction modes in VSC MTDC systems," in *Power and Energy Society General Meeting (PESGM)*, Boston, MA, USA, 2016.
- [19] "MathWorks," [Online]. Available: <https://se.mathworks.com/products/simulink/features.html#simulating-the-model>. [Accessed 23 May 2017].

Appendix

Appendix A: Matlab scripts and functions

A1 Basic scripts, *cable_paramters*, *cable_admittance_matrix* and *polar2complex*

A2 *cable_efficiency_var_cable_length*

A3 *cable_efficiency_var_alpha*

A4 *opt_V_scaling*

A5 *initiate_200km_cable_sim*

A6 Matlab function for the variable operation voltage model

Appendix B: Results from simulations

B1 Results of tuning the inner current controller

B2 Calculated cable efficiency

Appendix A: Matlab scripts and functions

Appendix A1

```
%cable_parameters
f = 50; %frequency [Hz]
V2 = 220e3; %nominal voltage [V]
Vmax = 1.1*220e3; %max voltage [V]
%A = 1000; %cable section [mm^2]
R = 0.048; %resistance [ohm/km]
L = 0.37e-3; %inductance [H/km]
C = 0.18e-6; %capacitance [F/km]
G = 0; %conductance [S/km]
Imax = 1055; %nominal current[A]

%cable_admittance_matrix
w = 2*pi*f; %angular speed
Z = R + 1i*w*L; %series impedance
Y = G + 1i*w*C; %shunt admittance
Zc = sqrt(Z/Y); %surge impedance
gamma = sqrt(Z*Y); %propagation constant
A = (coth(gamma.*l))/Zc; %matrix value A
B = -1./(Zc.*sinh(gamma.*l)); %matrix value B
II = [A, B; B, A]; %cable admittance matrix

%polar2complex
theta = deg2rad(b);
[Ex,Ey] = pol2cart(theta, a);
E = Ex+1i.*Ey;
```

Appendix A2

```
%cable_efficiency_var_cable_length
a = 1; %set alpha-value
b = 0:0.1:40; %varying beta-value
polar2complex %ref polar2complex
cable_parameters %refcable_parameters

%for loop calculating admittance matrix for cable lengths
for l = [100; 200; 300; 400] %cable lengths [km]
cable_admittance_matrix %ref cable_admittance_matrix
end

n = -real(conj(E.*B+A))./real(E.*conj(E.*A+B)); %efficiency calculation

%figure plot
plot(b,n)
xlabel('\beta [deg]')
ylabel('Cable efficiency')
legend('100 km', '200 km', '300 km', '400 km')

%scaling
xlim([0,40])
ylim([0.7,1])
```

Appendix A3

```
%cable_efficiency_var_alpha
l = 200; %cable length [km]
b = 0:0.1:10; %varying beta-value
cable_parameters %ref cable_parameters

%for loop calculating admittance matrix for alpha-values
for a = [1.000; 1.025; 1.050; 1.075; 1.100]; %varying alpha-value
cable_admittance_matrix %ref cable_admittancece
matrix
end
polar2complex %ref polar2complex

%efficiency calculation
n = -real(conj(E.*II(2)+II(1)))./real(E.*conj(E.*II(1)+II(2)));

%figure plot
plot(b,n)
xlabel('\beta [deg]')
ylabel('Cable efficiency')
legend('\alpha=1.000', '\alpha=1.025', '\alpha=1.050', '\alpha=1.075',
'\alpha=1.100')

%Set limits
xlim([0,10])
ylim([0.9,0.941])
```

Appendix A4

```
%opt_V_scaling

%Step 1 and 2
l = 200; %selected cable length
cable_parameters %ref cable_parameters
cable_admittance_matrix %ref cable_admittance_matrix

%Step 3

%fmincon function
x0 = [0,0]; %initial alpha- and beta-value
A = [];
b = [];
Aeq = [];
beq = [];
lb = [1,-pi/2]; %lower limit alpha- and beta-value
ub = [1.1,pi/2]; %upper limit alpha- and beta-value
fun = @ (x) (1-((-
real(conj((x(1)*exp(i*x(2)))*II(2)+II(1)))/real((x(1)*exp(i*x(2)))*conj((x(
1)*exp(i*x(2)))*II(1)+II(2))))))
nonlcon = @circlecon;
x = fmincon(fun, x0, A, b, Aeq, beq, lb, ub, nonlcon);

E = x(1)*exp(i*x(2)); %voltage scaling
n = -real(conj(II(2)*E+II(1)))/real(E*conj(II(1)*E+II(2))) %efficiency

[theta,rho] = cart2pol(real(E),imag(E));
b = rad2deg(theta);
e = rho+1i*b

%function for the cable efficiency limitation
function [c,ceq] = circlecon(x)
l = 200; %selected cable length
cable_parameters
cable_admittance_matrix
c = [((-
real(conj((x(1)*exp(i*x(2)))*II(2)+II(1)))/real((x(1)*exp(i*x(2)))*conj((x(
1)*exp(i*x(2)))*II(1)+II(2)))))-1,-((-
real(conj((x(1)*exp(i*x(2)))*II(2)+II(1)))/real((x(1)*exp(i*x(2)))*conj((x(
1)*exp(i*x(2)))*II(1)+II(2)))))]
ceq = [];
end
```

Appendix A5

```
%initiate_200km_cable_sim

l = 200; %cable length [km]
%Nominal values
Vn = 220e3; %nominal voltage
In = 1055; %nominal current
R = 1*0.048; %nominal resistance
L = 1*0.37e-3; %nominal inductance

%Base values
fb = 50; %base frequency
wb = 2*pi*fb; %base angular speed
Vb = (sqrt(2)/sqrt(3))*Vn; %base voltage
Ib = sqrt(2)*In; %base current
Sb = (3/2)*Vb*Ib; %base apparent power
Zb = Vb/Ib; %base resistance
Lb = Vb/(wb*Ib); %base inductance

%Per-unit values
wpu = 1; %per-unit angular speed
Lpu = L/Lb; %per-unit inductance
Rpu = R/Zb; %per-unit resistance

%Tuning of ICC
E = 1/sqrt(2); %damping
fsw = 2e3; %switching frequency
te = (3/2)*(1/fsw); %delay of pulse modulator
Ki_ICC = 1/(4*te*E^2) %integral gain ICC
Kp_ICC = Ki_ICC*(Lpu/(wb*Rpu)) %proportional gain ICC

%Tuning of OPC
Ki OPC = 1000; %integral gain OPC
Kp OPC = 1e-3; %proportional gain OPC
```

Appendix A6

```
function [V2a, V2b, V2c] = fcn(Pgrid)

%Cable parameters
f = 50;                %frequency [Hz]
R = 0.048;            %resistance [ohm/km]
L = 0.37e-3;          %inductance [H/km]
C = 0.18e-6;          %capacitance [F/km]
G = 0;                %[S/km]
l = 200;              %cable length [km]

%Calculation of cable terminal admittance matrix
w = 2*pi*f;           %
Z = R + 1i*w*L;       %series impedance
Y = G + 1i*w*C;       %shunt admittance
Zc = sqrt(Z/Y);       %
gamma = sqrt(Z*Y);    %
A = (coth(gamma.*l))/Zc; %
B = -1./(Zc.*sinh(gamma.*l)); %

x = [1.0313, 0.0785];

%Voltage controll
if Pgrid > 0
V2a = sqrt(2)*(sqrt(-Pgrid/(sqrt(3)*real(conj(B*(x(1)*exp(i*x(2)))+A))))))
V2b = sqrt(2)*(sqrt(-Pgrid/(sqrt(3)*real(conj(B*(x(1)*exp(i*x(2)))+A))))))
V2c = sqrt(2)*(sqrt(-Pgrid/(sqrt(3)*real(conj(B*(x(1)*exp(i*x(2)))+A))))))
else
V2a = 220e3
V2b = 220e3
V2c = 220e3
end

V2 = [V2a, V2b, V2c];
```


Appendix B: Results from simulations

Appendix B1

Fig. 41 and Fig. 42 show the alignment between the control current and reference current for i_d and i_q with constant reference value equal to 1.0 and zero respectively.

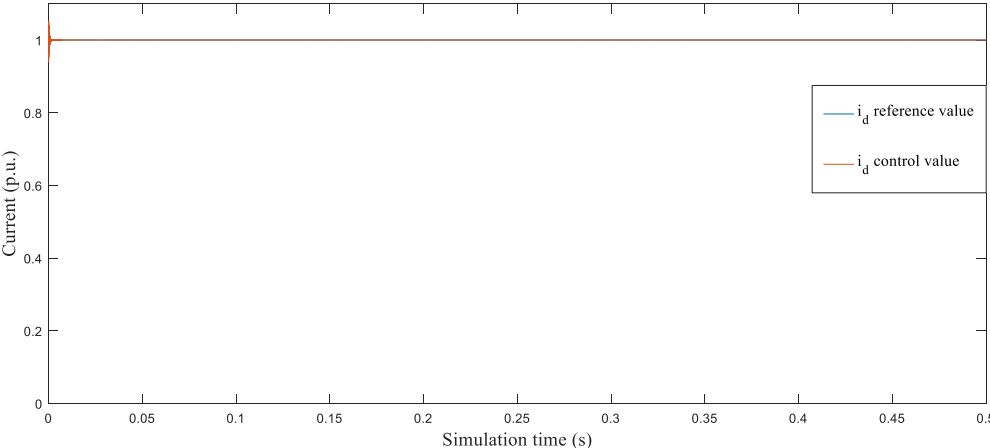


Fig. 41. Alignment for constant reference current equal to 1.0 p.u. and control current, i_d .

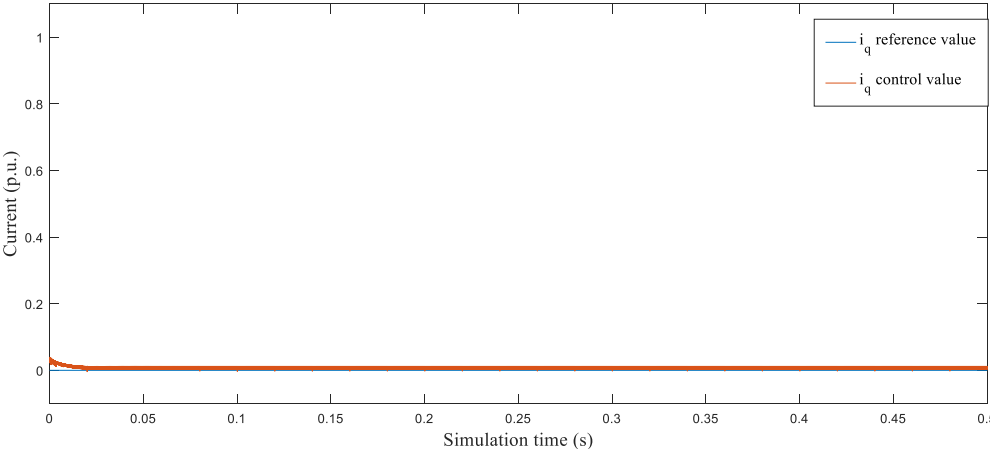


Fig. 42. Alignment for constant reference current equal to 1.0 p.u. and control current, i_q .

Fig. 43 and Fig. 44 show the alignment between the control current and reference current for i_d and i_q with varying reference value 0.3-1. p.u. current.

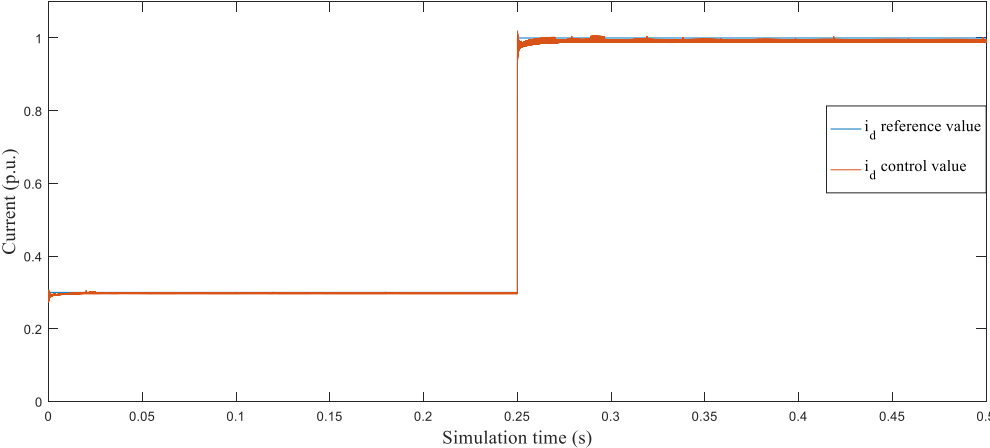


Fig. 43. Alignment for varying reference current (0.3-1.0 p.u.) and control current, i_d .

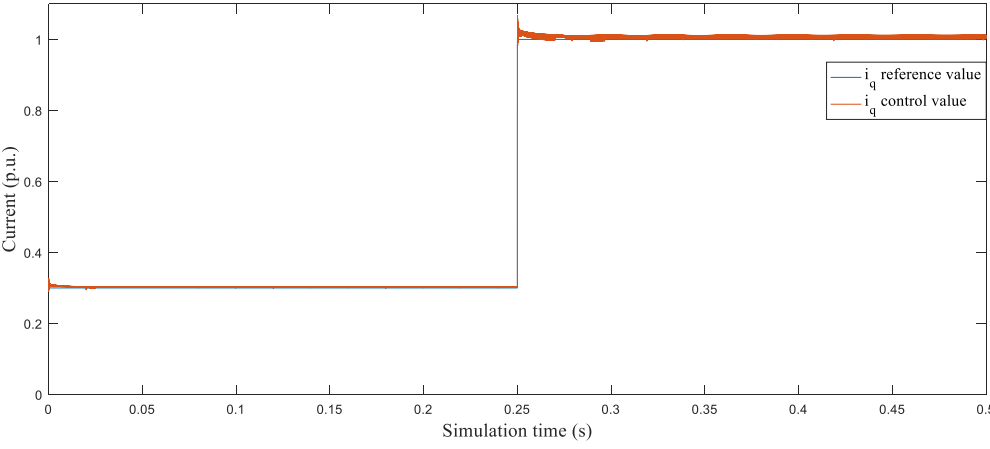


Fig. 44. Alignment for varying reference current (0.3-1.0 p.u.) and control current, i_q .

Fig. 45 and Fig. 46 show the alignment between the control current and reference current for i_d and i_q with varying reference value 0.3-1. p.u. for i_d and reference value for i_q set as constant zero.

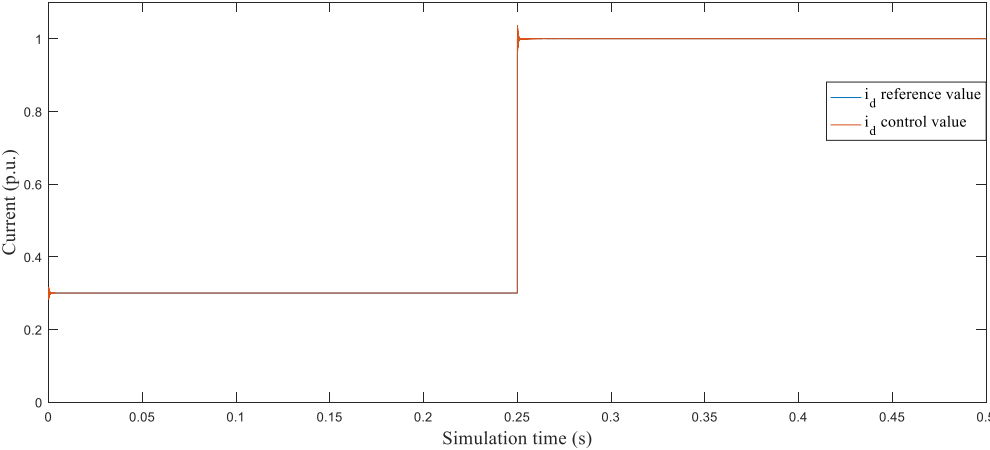


Fig. 45. Alignment for varying reference current (0.3-1.0 p.u.) and control current, i_d . With reference i_q set at constant value equal to zero.

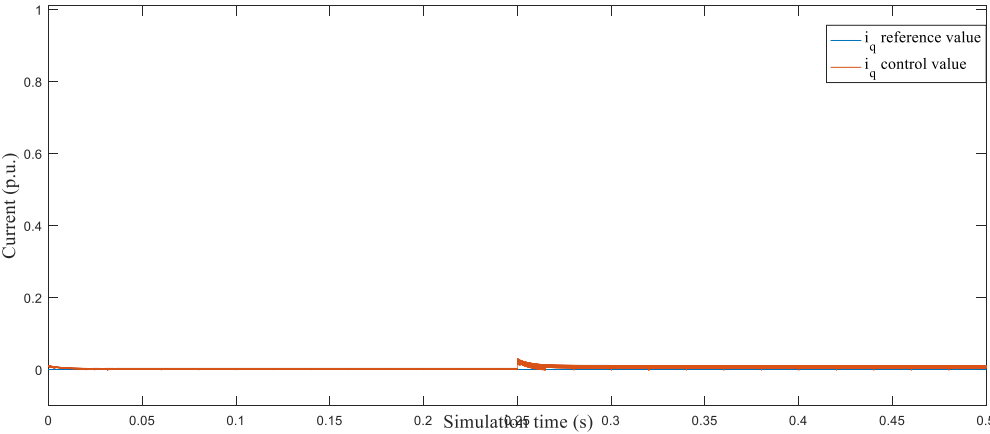


Fig. 46. Alignment for constant reference current equal to zero and control current, i_q . With varying reference current i_d (0.3-1.0 p.u.).

Appendix B2

TABLE VII and TABLE VIII show the calculated efficiencies for the fixed and variable operation voltage model simulations respectively. The numbers marked in red represents the simulations were the operation current of the cable has exceeded the cable's rated current.

TABLE VII. Calculated cable efficiency for fixed operation voltage model simulation. The red numbers mark the simulations where the current exceeds the cable's current limit.

Power	0.1 p.u. voltage	0.2 p.u. voltage	0.3 p.u. voltage	0.4 p.u. voltage	0.5 p.u. voltage	0.6 p.u. voltage	0.7 p.u. voltage	0.8 p.u. voltage	0.9 p.u. voltage	1 p.u. voltage
0.1 p.u.	0.825	0.871	0.790	0.654	0.474	0.251	-0.014	-0.321	-0.669	-1.057
0.2 p.u.	-0.050	0.876	0.865	0.808	0.723	0.615	0.484	0.332	0.159	-0.035
0.3 p.u.	-0.046	0.855	0.879	0.853	0.802	0.733	0.648	0.548	0.433	0.305
0.4 p.u.	-0.035	0.825	0.879	0.871	0.838	0.790	0.728	0.654	0.570	0.474
0.5 p.u.	-0.025	0.783	0.873	0.878	0.858	0.822	0.775	0.717	0.650	0.575
0.6 p.u.	-0.018	-0.085	0.864	0.880	0.869	0.842	0.805	0.758	0.704	0.641
0.7 p.u.	-0.013	-0.064	0.853	0.879	0.875	0.856	0.826	0.787	0.741	0.688
0.8 p.u.	-0.010	-0.056	0.840	0.876	0.879	0.865	0.840	0.808	0.769	0.723

TABLE VIII. Calculated efficiency for the simulation of the variable operation voltage model. The red number mark the simulations where the current exceeds the cable's current limit.

Power	Efficiency	p.u. voltage
0.1 p.u.	0.846	0.242
0.2 p.u.	0.846	0.341
0.3 p.u.	0.846	0.418
0.4 p.u.	0.846	0.482
0.5 p.u.	0.846	0.539
0.6 p.u.	0.846	0.590
0.7 p.u.	0.846	0.637
0.8 p.u.	0.846	0.681